Progress in Oceanography 82 (2009) 81–100

Contents lists available at ScienceDirect

Progress in Oceanography

journal homepage: www.elsevier.com/locate/pocean

The 2004–2008 mean and annual cycle of temperature, salinity, and steric height in the global ocean from the Argo Program

Dean Roemmich *, John Gilson

Scripps Institution of Oceanography, University of California San Diego, 9500 Gilman Drive, La Jolla, CA 92093-0230, USA

ARTICLE INFO

Article history:
Received 3 June 2008
Received in revised form 16 March 2009
Accepted 29 March 2009
Available online 11 April 2009

ABSTRACT

The Argo Program has achieved 5 years of global coverage, growing from a very sparse global array of 1000 profiling floats in early 2004 to more than 3000 instruments from late 2007 to the present. Using nearly 350,000 temperature and salinity profiles, we constructed an upper-ocean climatology and monthly anomaly fields for the 5-year era, 2004–2008. A basic description of the modern upper ocean based entirely on Argo data is presented here, to provide a baseline for comparison with past datasets and with ongoing Argo data, to test the adequacy of Argo sampling of large-scale variability, and to examine the consistency of the Argo dataset with related ocean observations from other programs. The Argo 5-year mean is compared to the World Ocean Atlas, highlighting the middle and high latitudes of the southern hemisphere as a region of strong multi-decadal warming and freshening. Moreover the region is one where Argo data have contributed an enormous increment to historical sampling, and where more Argo floats are needed for documenting large-scale variability. Globally, the Argo-era ocean is warmer than the historical climatology at nearly all depths, by an increasing amount toward the sea surface; it is saltier in the surface layer and fresher at intermediate levels. Annual cycles in temperature and salinity are compared, again to WOA01, and to the National Oceanography Center air–sea flux climatology, the Reynolds SST product, and AVISO satellite altimetric height. These products are consistent with Argo data on hemispheric and global scales, but show regional differences that may either point to systematic errors in the datasets or their syntheses, to physical processes, or to temporal variability. The present work is viewed as an initial step toward integrating Argo and other climate-relevant global ocean datasets.

1. Introduction

Descriptions of the global ocean's large-scale temperature and salinity distributions and circulation have always been severely limited by the sparseness of the underlying datasets. Until recently, subsurface data could not be collected over whole ocean basins simultaneously, so historical datasets have strong regional and seasonal biases. The best available syntheses of the subsurface ocean, such as the World Ocean Atlas series (e.g. WOA01, Conkright et al., 2002) have by necessity been compiled using regional datasets from different eras. These "mixed-era" climatological fields have many important applications, but they do not represent the time mean ocean over a given period, and thus are problematic for assigning error bounds (e.g. Roemmich and Sutton, 1998). Even the ambitious World Ocean Circulation Experiment's (WOCE) global hydrographic survey sampled different oceans in different years and left vast gaps of thousands of kilometers between widely spaced ship tracks.

The interpretation problems posed by historical subsurface ocean datasets go beyond simple sparseness. The data are very inhomogeneous in space and time. They have strong biases toward the northern hemisphere oceans and toward developed nations' coastlines. There are far more summer data than winter data in the archives, and data collected south of 30°S in winter are especially rare (Fig. 1.1).

The implications of such inhomogeneous sampling, in turn, go beyond the difficulty of defining climatological fields. Since the mean for any given decade is poorly sampled, so the estimation of decadal and multi-decadal variability is subject to large errors. For example, estimates of the 50-year increase in steric sea level and ocean heat content (Levitus et al., 2005a; Ishii et al., 2006) may be biased low by up to 100% (Gregory et al., 2004; Gille, 2008) because the objective analysis technique used in these studies estimates zero anomaly in unsampled regions. Climatologies are widely used in prognostic and data assimilation models for initialization and to limit unrealistic variability. Their deficiencies as representations of the mean state can affect those models significantly, for example, by creating spurious signals where new observations are inconsistent with the previous estimate of the mean. A further complication with some climatologies based on historical datasets is their reliance on multiple instrument types. Recent work has highlighted significant biases that result from mixing XBT and hydrographic data (Gouretski and Koltermann, 2007; Willis et al., 2007; Wijffels et al., 2008), including

* Corresponding author. Tel.: +1 858 534 2307; fax: +1 858 534 9820.
E-mail address: droemmich@ucsd.edu (D. Roemmich).

0079-6611/$ - see front matter © 2009 Elsevier Ltd. All rights reserved.
doi:10.1016/j.pocean.2009.03.004

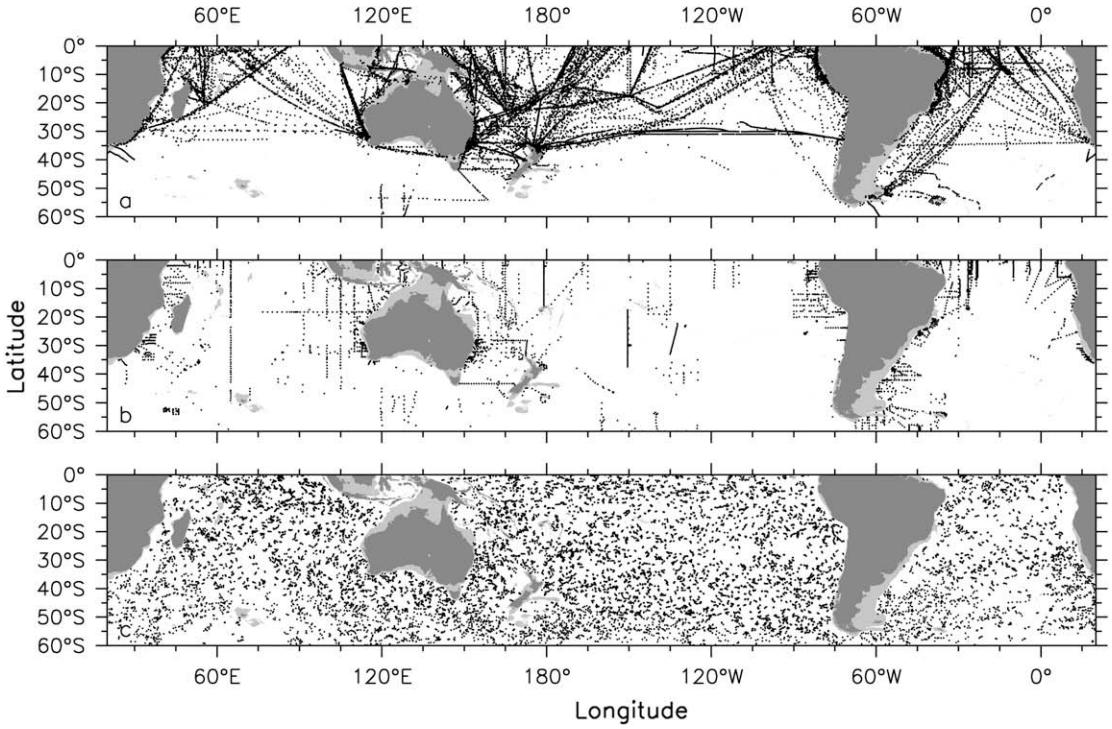

Fig. 1.1. (a) Locations of 24,175 southern hemisphere XBT temperature profiles for all years prior to 2001 with data to 300 m or deeper. (Source World Ocean Database.) (b) Locations of 3186 hydrographic station for August in the years 1951–2000, including all those with temperature and salinity to at least 1000 m. (Source: World Ocean Database.) (c) Locations of 28,183 southern hemisphere Argo profiles for August from 2004 to 2008.

impacts on estimated decadal variability in ocean heat content (Domingues et al., 2008).

The technology of autonomous profiling floats has made it possible to sample the subsurface oceans globally, and the Argo Program was initiated (Roemmich et al., 1998) to exploit float technology for that objective. This work presents a "fixed-era" single-instrument climatology for the global upper ocean, in contrast to the previous "mixed-era", and often multi-instrument, climatologies. The fixed-era climatology is the temporal mean over the period 2004–2008, based on the Argo dataset. Beyond simply describing the time mean fields and the annual variability, the value of the fixed-era ocean climatology is illustrated with a few comparative examples. A primary objective is to provide a baseline against which both ongoing Argo data and past datasets can be compared for estimates of interannual-to-decadal variability. Another objective is to begin integrating the global ocean observing system by comparing Argo to related global datasets such as air–sea fluxes, sea surface temperature, and satellite altimetric height. The present work is a first effort, and the accuracy of Argo-based multi-year mean fields will continue to progress with time and with improvements in the number, distribution, and data quality of Argo floats.

The Argo dataset greatly reduces the sampling biases noted above in historical hydrographic data. In the present work, 345,902 Argo temperature–salinity–pressure profiles are used from the period January 2004 to December 2008. The 2004 starting point was chosen as the first year that Argo achieved sparse global coverage. Of the total stations, 29% are south of 30°S, and one-fourth (24.8%) of those are from the winter months July to September. The 5-year Argo dataset has many times the number of Southern Ocean winter temperature/salinity stations obtained in the entire pre-Argo history of oceanography (Fig. 1.1), and the regional and seasonal biases are greatly reduced.

Some sampling problems remain, presenting challenges to the Argo Program for future improvements. During the 5-year period, the number of Argo floats tripled to more than 3000, with greatly increased coverage in some regions. Because the coverage was changing during the 5-year averaging period, there is a degree of ambiguity in separating seasonal and longer-term variability. There are few Argo floats in most marginal seas and few, but increasing, floats in seasonally ice-covered regions. The latter limits the effective coverage of the array to about 60°S to 65°N. Due to present limitations on buoyancy adjustment, some floats in the tropics do not sample below 1000 dbar. Finally, a northern hemisphere bias still exists. In the 5-year dataset, the average number of profiles per unit area of ocean deeper than 2000 m is about 40% greater in the northern hemisphere than the southern hemisphere. Another objective of the present work is to illustrate the need for continuing expansion of the well-sampled Argo domain, in profile depth and in spatial distribution of floats.

In the next section, the dataset and interpolation methods are described. Section 3 shows 5-year means of temperature, salinity, and steric height from Argo, and compares them with WOA01[1]. In Section 4, the annual cycle calculated from Argo is examined and compared for consistency with annual cycles in air–sea exchanges of heat and freshwater from the National Oceanography Center (NOC) Air–Sea Flux Climatology (Josey et al., 1998), sea surface temperature (Reynolds et al., 2002), and sea surface height from satellite altimetry (Ducet et al., 2000). These data products are all independent of Argo, but describe closely related quantities. Discussion and conclusions are presented in the final section.

2. Data and methods

The Argo profiles used in this study were those available from the Argo Global Data Assembly Center (GDAC) in early 2009. The

[1] WOA01 is used because later releases of the World Ocean Atlas include substantial amounts of Argo data.

dataset included 436,842 candidate profiles gathered during 2004–2008, with differing levels of quality control (QC) applied. New Argo data are available in a real-time quality controlled state (RTQC) having only automated QC procedures applied. Older data have delayed-mode quality control (DMQC) including a more rigorous examination by a scientist responsible for the Argo float. Data of both QC levels were used here, but with additional testing of the RTQC files. The Argo QC flags attached to the temperature and salinity profile values were used as a first pass quality assessment. The Argo climatology in the present work is based on a reduced subset of 345,902 profiles (Fig. 2.1a), a 20.8% reduction of the total available dataset. Some exclusions were for reasons of data quality (temporary or otherwise), while others were due to the choice of spatial domain for the present work. Specifically:

(1) Profiles (5.0%) were removed due to systematic pressure errors detected (e.g. Willis et al., 2007) in a subset of profiles from Woods Hole Oceanographic Institution (WHOI) SOLO floats equipped with Falmouth Scientific Instruments (FSI) Conductivity-Temperature-Depth (CTD) sensors. Some profiles from these floats have been corrected and are included. Regionally the reduction is more severe in the Atlantic Ocean, where most of the problematic floats are located, resulting in gyre-scale low coverage gaps in the Argo array (Fig. 2.1a), most notably between 10°N and 30°N and in the South Atlantic.

(2) Eligible profiles (5.0%) were excluded either because they fell outside the mapping domain or did not report a position. The present mapping domain (see Fig. 2.1a) excludes marginal seas, of which only a few have good Argo sampling. The data domain is further limited to 70°S to 67°N, excluding higher latitudes. Although data were included to 70°S, the gridded region ends at 60°S since the coverage further poleward is very sparse.

(3) Eligible profiles (2.3%) were rejected by comparing against the Argo 'greylist' of problematic instruments. This is in addition to greylisted WHOI FSI profiles discussed above.

(4) Profiles (4.3%) were rejected for not returning viable temperature and salinity values over a significant pressure range. This includes early-Argo-era temperature-only floats and entire profiles marked bad during QC.

(5) Adjustment for conductivity sensor drift, by comparing salinity values to a historical estimate (e.g. Wong et al., 2003; Owens and Wong, 2009), is a critical task of DMQC. RTQC profiles without the benefit of DMQC were adjusted here by an offset to agree with the WOCE Global Hydrographic Climatology (WGHC, Gouretski and Koltermann, 2004) salinity over the deepest portion of the profile. This procedure was judged to be insufficient, and the profile rejected, if the difference between the profile and WGHC was more than 0.1 psu (0.7%) or if the profile only extended to a pressure shallower than 600 dbar (1.5%).

Salinity adjustments were applied to about 140,000 RTQC profiles, with a negligibly small mean salinity adjustment (.00008 psu) and RMS of 0.022. In DMQC profiles, the deviations from historical salinity over most of the oceans decrease with depth, and are considerably smaller at 2000 dbar than in intermediate pressure layers. For this reason, we conclude that the T–S adjustments applied to RTQC profiles are mainly correcting for sensor drift, rather than canceling climatic T–S changes. The global T–S differences in Argo data relative to WOA01 at intermediate and upper levels, described in Section 3, are not very sensitive to the deep salinity adjustment applied to these profiles.

(6) Additional quality checks resulted in 2% of profiles being rejected. Reasons for rejecting whole profiles included low vertical pressure resolution, lack of QC flags applied within the Argo file, bad file formats, and density inversions greater than 0.01 kg/m^3 (0.05 kg/m^3) deeper (shallower) than 400 dbar. Density inversions less than 0.05 kg/m^3 were common shallower than 400 m, and not usually indicative of a bad profile. For these, the inverted levels were removed if

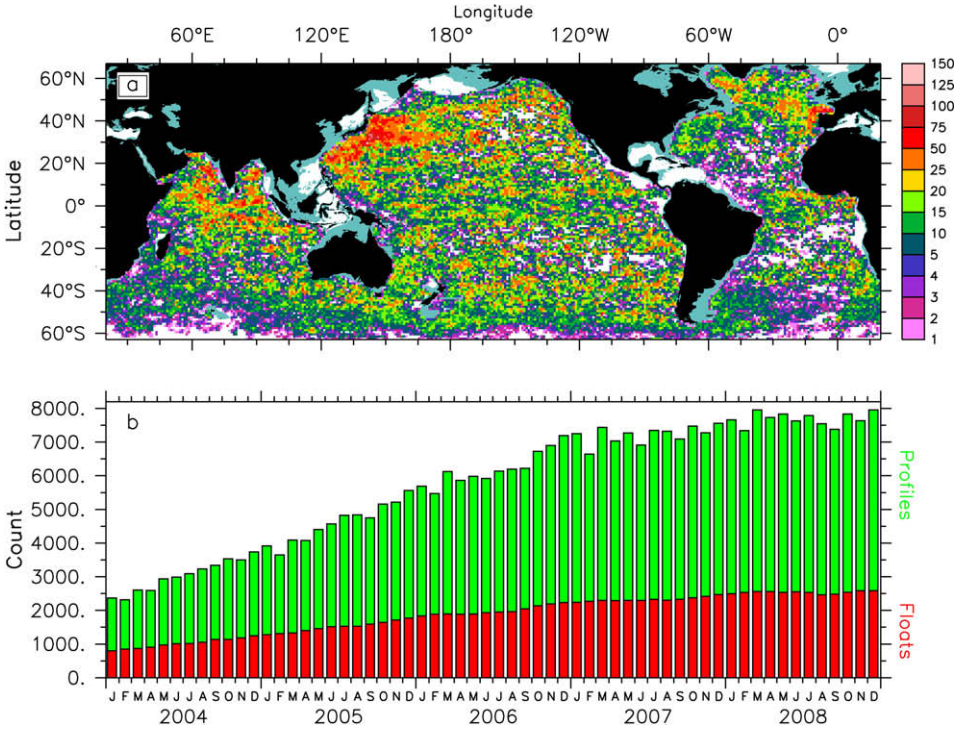

Fig. 2.1. (a) 1° × 1° binned count of Argo temperature and salinity profiles used in this analysis, January 2004–December 2008. (b) Monthly census of profiles (green) and floats (red) used in this analysis.

the shallow inversion was greater than .01 kg/m^3. For pressure inversions or "stalls", often indicative of grounded instruments, only levels below the stall or pressure inversion were removed.

The remaining Argo profile data were linearly interpolated onto 58 pressure levels spanning 0–2000 dbar, with separate levels spaced from 10 to 100 dbar apart. The shallowest sampled value, if above 15 dbar, was assumed to represent the near-surface value. In a few early-era Argo floats, the shallowest values were at 10 dbar, while newer floats tend to sample closer to the sea surface. Finally, on each pressure level the Argo profiles were compared to a local mean and variability in $10^\circ \times 10^\circ$ spatial boxes. If the value at any level differed from the mean by more than six standard deviations, the whole profile was excluded, resulting in an additional 0.1% of rejections.

Data coverage for shallow pressure levels is shown in Fig. 2.1a. Coverage decreases between 1000 and 2000 dbar in tropical oceans as some Argo float models cannot yet produce the buoyancy required to reach the sea surface from 2000 dbar in the highly stratified tropical oceans. At present, 731 out of 1159 active floats in the tropics profile below 1500 m.

The monthly number of Argo profiles and floats included in the Argo climatology has grown more than threefold from approximately 2300 monthly profiles (800 floats) in early 2004 to 7600 profiles (2600 floats) in late 2008 (Fig. 2.1b). As the Argo array has now reached its target of 3000 active floats, future growth in the monthly number of floats and profiles included in the climatology will occur due to inclusion of marginal seas and high latitudes in the study domain, increased float and CTD reliability, and continuing DMQC of the dataset.

In the present dataset, monthly southern hemisphere profiles have outnumbered those in the northern hemisphere since December 2004. In 2004–2005, large but diminishing coverage gaps existed in the southeast Pacific, South Atlantic, and Southern Oceans. Including all data from the 5-year span (Fig. 2.1a), there are still some smaller, unsampled areas of the open ocean. In addition to the gaps in the Atlantic and Southern Ocean, smaller gaps can be found in the eastern central ocean basins where floats tend not to move far from their deployment locations. Best coverage is found where float numbers and dispersion are both high, such as the Kuroshio Extension region and the northern Indian Ocean. Coverage in later months of the year (e.g. November, December) is slightly denser than early months (e.g. January, February) due to the 5-year continuous growth in the number of floats.

The dramatic contrast in coverage between Argo and historical data in the southern hemisphere is illustrated in Fig. 1.1 by profile locations shown for August XBT data (a), ocean station data (b), and Argo (c). One can see that the historical dataset in the southern hemisphere is very sparse, not sufficient for accurate estimation of an annual cycle globally, and especially sparse for salinity or deep temperature. Argo coverage constitutes a major increment over historical datasets.

For interpolation of the Argo temperature and salinity data, a 5-year mean field for each month was first estimated using a weighted least-squares fit to nearby data. Then, anomalies from this first estimate, for each of the 60 months of the time-series, were calculated by objective analysis. The weighted least-squares procedure was adopted after some experimentation, to arrive at a stable "first guess" of the mean field. The fact that results have some sensitivity to the procedure indicates that 5 years of Argo data still leaves significant uncertainty in the mean field (see Section 3.3 on errors).

The weighted least-squares "first guess" fit included linear and quadratic terms in latitude, longitude, and pressure (as in Ridgway et al., 2002), and was carried out separately at each pressure level. Six temporal harmonics (i.e. periods of 2–12 months) were included to permit an irregular annual cycle. A total of 300 "nearest" points were used for each fit, 100 from the present pressure level plus 100 from each adjacent pressure level above and below, for each of the 12 months. Data were weighted in inverse proportion to their horizontal distance from the grid point, with the nearest data point receiving a weight of 1 and the most distant a weight of 0.02.

For both the least-squares fit and the subsequent objective analysis of anomalies, the horizontal distance between data and grid points was increased by an amount proportional to the difference in ocean depth. This is similar to a penalty for crossing contours of barotropic potential vorticity, f/H. Our depth scaling is similar to that used by Lavender et al. (2005). This extra term improved the representation of narrow topography-following features such as western boundary currents, which may have relatively few data on their inshore sides. Hence:

$$\text{distance} = \text{sqrt}\left(\text{dist}_y^2 + \text{dist}_x^2 + \text{dist}_H^2\right) \quad (1)$$

where dist_x (dist_y) is the horizontal distance in km in the zonal (meridional) direction, and dist_H is the added distance penalty (km) for crossing H contours, calculated as

$$\text{dist}_H = 200\ \text{km} \cdot 5^{1/2} \cdot [H_\text{d} - H_\text{g}] / \left[H_\text{d}^2 + H_\text{g}^2\right]^{1/2}$$

with the subscripts d and g referring to H evaluated at data and grid points, respectively. This scaling equates a doubling of H with a distance of 200 km. Finally, distance was considered to be infinite between ocean locations separated by continental land, such as southern India, or by substantial islands including New Zealand, Madagascar, and Tasmania.

The first estimate by least-squares fit worked well for grid points surrounded by nearby data, and less well in regions where data were predominantly on one side of the grid point and far away, causing unstable extrapolations. We discarded the fit in cases where the estimated value of temperature or salinity was outside the data envelope, replacing it with the corresponding data extremum. These extrapolation problems occurred mostly in the data-sparse Southern Ocean. Finally, after fitting all pressure levels, density inversions occurred occasionally in upper waters. These were eliminated by adjusting temperature and salinity of shallower layers to remove unstable density differences relative to deeper values, if greater than .01 kg/m^3. The net effect was a small mean positive offset in temperature by .015 °C at the sea surface, decreasing to 0.0002 °C at 100 m. The quality of the first-estimate mean field is a concern.

After making the initial estimate of the 5-year mean for each month, the 60 monthly anomaly fields were then calculated using objective analysis (Bretherton et al., 1976; see also Roemmich, 1983, for an example using hydrographic data). For the objective analysis, the spatial covariance of the monthly data anomalies was represented with functions that approximate the normalized sample covariance (Fig. 2.2a). The sample covariance was formed by subtracting the first-estimate monthly mean field, linearly interpolated to Argo profile locations in space and time, and then averaging the covariance estimates as a function of distance separation (as defined above) globally and over the 60-month record.

For the objective analysis, which was done separately for each month and pressure level, the normalized spatial signal covariance of temperature and salinity was represented as the sum of a small-scale Gaussian function and a large-scale exponential (Fig. 2.2b):

$$C(x) = 0.77\exp(-(a*\text{distance}/140)^2) + 0.23\exp(-|a*\text{distance}|/1111)$$

where the distance (km) is defined by (1). This function is similar to that used by Willis et al. (2004) to simulate the universal altimetric

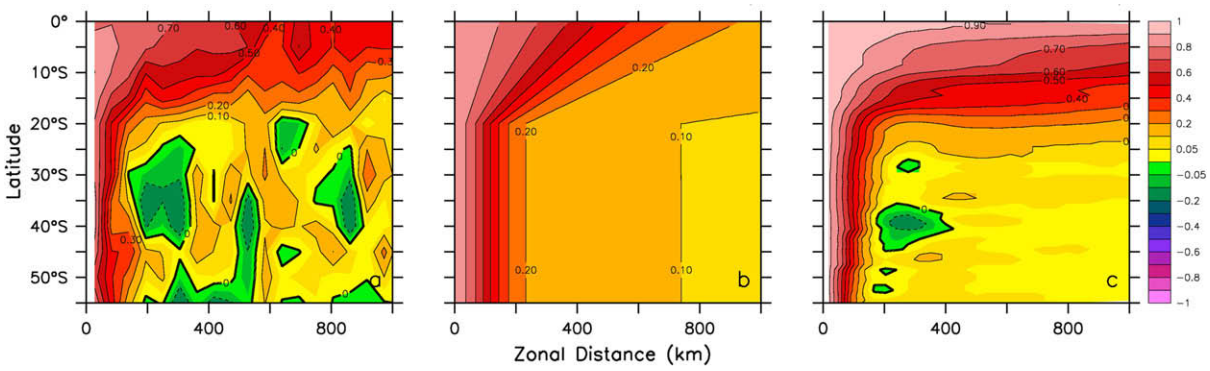

Fig. 2.2. The normalized zonal covariance of steric height (0/800 dbar) anomalies, as a function of latitude, (a) estimated from 5 years of Argo data (2004–2008), (b) as approximated in functional form for objective analysis of temperature and salinity fields , and (c) estimated from the 15-year (1993–2007) AVISO satellite altimetry product.

height spectrum proposed by Zang and Wunsch (2001). In order to represent the zonal elongation of correlation in the tropics, ($dist_x$, $dist_y$, $dist_H$) are scaled by a factor of $a = (1, 1, 1)$ for latitudes poleward of 20°, and decreasing linearly to $a = (.25, 1, 1)$ for latitudes equatorward of 20° (Fig. 2.2b). Finally, the noise-to-signal variance ratio (added to the main diagonal of the data covariance matrix) was taken to be 0.15. The anomaly fields were added to the first-estimate means to form the final 60 monthly estimates.

Fig. 2.2 shows both the sample covariance, based on steric height anomaly (0/800 dbar), and the modeled one. In order to illustrate the zonal stretching in the tropics, this is shown for zonal lags only, based on pairs of profiles that are separated in time by less than 1 day and latitude by less than 0.5°. The model function is a good representation of the sample covariance in the tropics and at short lags in middle latitudes. It appears to overestimate the correlation at longer scales in middle latitudes.

Fig. 2.2 also shows, for illustrative purpose, the zonal covariance of altimetric height anomaly, 1993–2007, relative to the 15-year mean, based on the gridded AVISO dataset. The altimetric height covariance is similar to that of steric height, but an important point is that as the record length increases with time, interannual and decadal variability raises the large-spatial-scale portion of the sample covariance (see also Fig. 3.9). Previous studies of spatial correlation of temperature anomalies from XBT datasets (e.g. White, 1995) indicate higher correlation at large spatial lags in middle latitudes than seen in Fig. 2.2, and this is partly attributable to the longer-term mean used in those studies. Evaluation of the effectiveness of Argo for sampling large-scale ocean variability should take into account that the signal level will continue to increase with the length of the global time-series.

The interpolation procedures described above use simplified representations of the ocean's temporal mean and its statistics of variability. While the objective is to produce an accurate climatology for the Argo era, the relatively small volume of data to date, and uncertainties in the statistics of the fields, make an *ad hoc* mapping procedure necessary. We sought consistency with the statistics indicated by the data, and have tried several different plausible choices. Alternate or more complicated approaches did not reduce the mapping errors as estimated in Section 3.3 below. Nevertheless, the maps will clearly improve with time as the growing Argo dataset contributes to the background mean field and to more accurate statistics of variability.

3. The 2004–2008 mean

The 5-year Argo time-averaged fields of temperature and salinity versus pressure were obtained by averaging the monthly fields, including the first-estimate and the monthly anomalies, over the 60-month period. Additionally, the monthly temperature and salinity fields were used to calculate potential density, steric height, and geostrophic velocity. These derived quantities in turn were also averaged over the 60-month period. In calculations of zonally or globally averaged quantities, pressure levels deeper than the mean depth of a $1° \times 1°$ grid box were masked out. In addition, grid points near continental coastlines and large islands were masked out at all depths if the average depth in the $1° \times 1°$ grid box was less than 500 m, because these inshore extrapolated values tended to have large estimation errors (Section 2).

3.1. Temperature, salinity, and density

In order to compare temperature, salinity, and density from the Argo climatology to that of WOA01 (Conkright et al., 2002), the latter product was masked to the same grid point locations as Argo, eliminating marginal seas and shallow regions. The depth coordinate in WOA01 was converted to pressure, and linearly interpolated onto the same pressure surfaces used for Argo. Fig. 3.1 shows contours of zonally averaged temperature, salinity, and density from Argo, as a function of pressure. Color shading is used to show the differences, Argo-minus-WOA01. Fig. 3.2 shows maps of temperature, salinity, and density, vertically averaged over the top 100 dbar, again with contour lines for Argo and color shading for Argo-minus-WOA01 differences. The differences include sampling and interpolation errors as well as decadal changes.

The zonally averaged temperature (Fig. 3.1a) shows bands of warming extending deep into the ocean in Argo-minus-WOA01 differences in both hemispheres at middle and high latitude. These differences are generally consistent with the linear trends found by Levitus et al., 2005a. The area of the northern hemisphere oceans north of 40°N is much smaller than that of southern hemisphere oceans south of 40°S. Thus, although the zonally averaged temperature increase is greater in the north, it represents a much smaller difference in total heat content than the southern hemisphere signal. In addition to these signals which extend to depth, the surface layer is warmer in Argo than in WOA01 at nearly all latitudes. Surface layer warming is greatest in the Atlantic (Fig. 3.2a). When volume-averaged globally from 0 to 2000 dbar, the Argo climatology is 0.036 °C warmer than WOA01, with maxima in area-averaged temperature difference at the sea surface and about 1000 dbar (Fig. 3.3).

In zonally averaged salinity (Fig. 3.1b), the northern hemisphere ocean is generally saltier in Argo than in WOA01, while the southern hemisphere ocean is mostly fresher. The southern freshening signal is seen as a tongue of negative salinity difference extending from the sea surface at high southern latitudes into the ocean interior and northward at intermediate depth. This freshening is

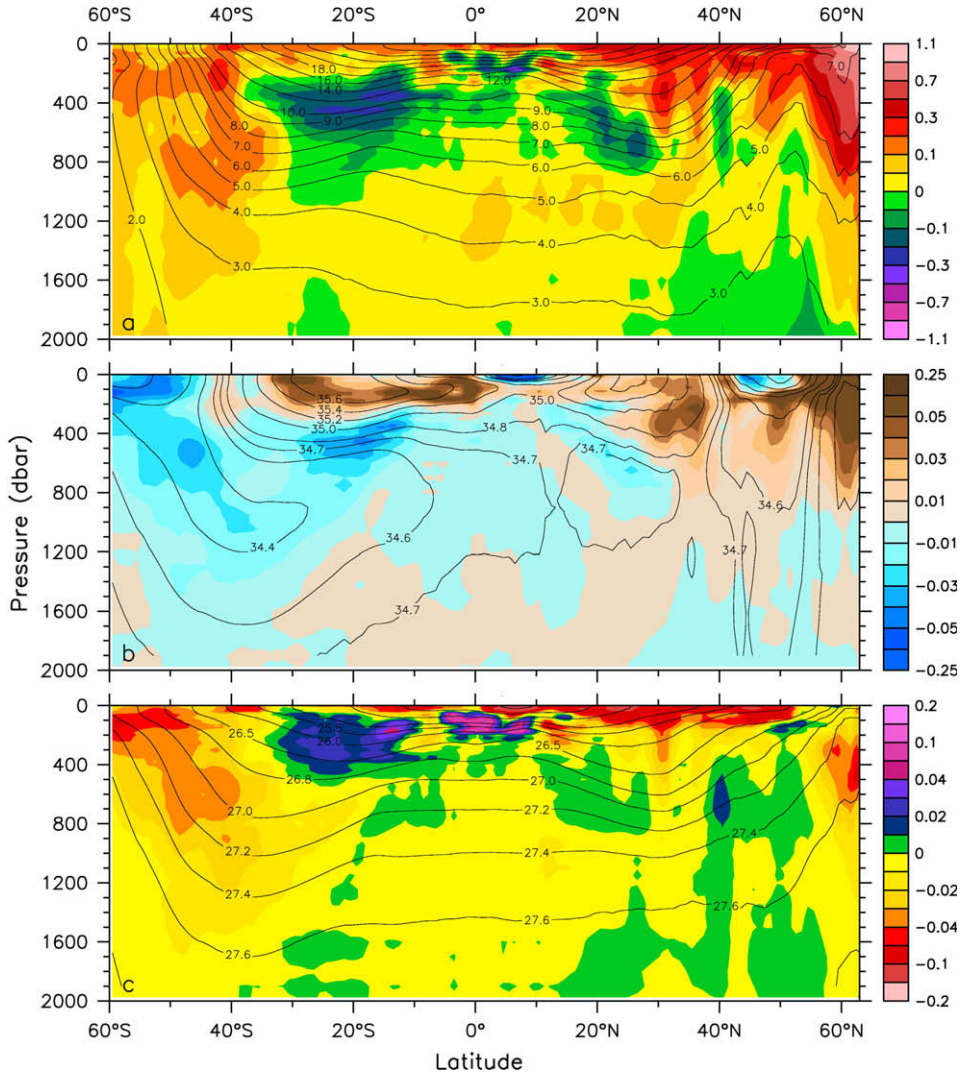

Fig. 3.1. (a) Zonally averaged temperature (°C) versus pressure for the Argo 5-year mean (contours) and Argo-minus-WOA01 difference (color shading). (b) Same as (a) except for salinity. (c) Same as (a) except for density (σ_θ).

consistent with previous comparisons of modern and historical data by Wong et al. (1999) in the Pacific and Indian Ocean and by Curry et al. (2003) in the Atlantic. In Argo compared to WOA01, the southern freshening is seen in all three oceans. The salinity increase in the north is dominated by the Atlantic Ocean, and occurs mainly north of 40°N. This has been previously noted by Hatun et al. (2005), with the increase occurring during the past decade. In addition to these deeper salinity signals, there are surface layer changes (Figs. 3.1b and 3.2b) including salinity increases in the evaporative regions of 20°–40°N and S in all oceans. The Argo-era surface layer of the Atlantic is saltier in both hemispheres (Fig. 3.2b, colors), suggesting decreased precipitation-minus-evaporation (P − E) in that ocean, and balanced largely by freshening in the Pacific. A strong surface freshening signal is seen, centered at 7°N (Fig. 3.1b), near the salinity minimum that lies beneath the Inter-Tropical Convergence Zone (ITCZ). Fig. 3.2b shows pronounced freshening in the west under both the Pacific ITCZ and the South Pacific Convergence Zone. These signals may in part be due to a preponderance of La Niña conditions in the Pacific during the Argo era.

The volume-averaged 0–2000 dbar Argo climatology is .002 fresher than WOA01, with area averages showing a shallow salinity increase with maximum at about 100 dbar (Fig. 3.3) and deeper salinity decrease with maxima at 500 and 1000 dbar. The mean salinity decrease above the density surface σ_θ equals 27.6 is also .002 psu, equivalent to dilution of the water column by 8 cm of fresh water. Averaging above a density surface is done to exclude the vertical displacement of density and salinity from the estimate. This net freshening may not be significant given that Argo salinity quality control is not yet completed for the 2004–2008 period. As a climate signal, the freshening would include contributions from the melting of both continental ice and floating ice over the period of a few decades between the WOA01 and Argo eras.

The zonally averaged density differences (Fig. 3.1c) reflect the north/south asymmetry in salinity difference. That is, in the Southern Ocean the freshening signal reinforces the warming, with both causing density to decrease. But in the 40–50°N band, the salinity increase tends to cancel the warming signal, and a small density increase is seen at all depths below the surface layer. Hence, while substantial deep temperature increases are seen at high latitude in both hemispheres (Fig. 3.1a), the corresponding density decrease is greater in the southern hemisphere. This point is reinforced in the next section below on steric height. Opposing northern trends in thermosteric height and halosteric height, again deriving from the North Atlantic, have also been shown by Levitus et al. (2005b).

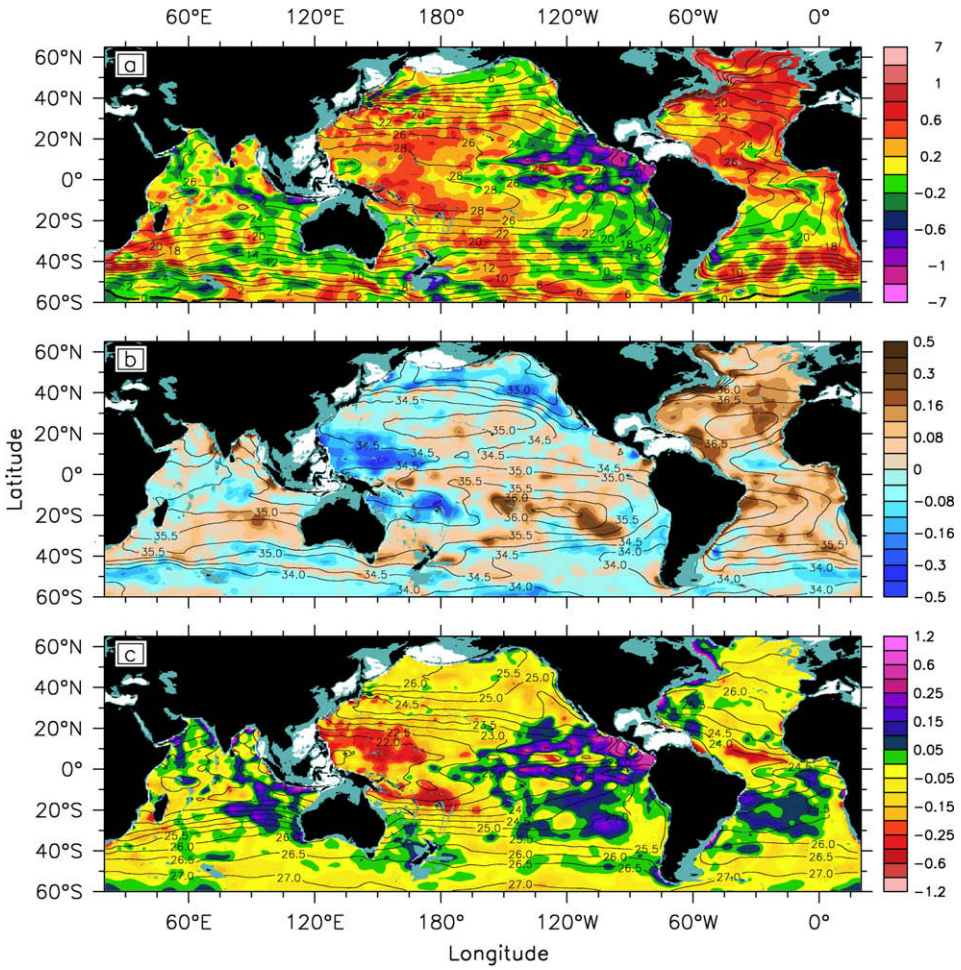

Fig. 3.2. (a) Map of 0–100 dbar vertically averaged temperature (°C) from the Argo 5-year mean (contours) and Argo-minus-WOA01 difference (color shading). (b) Same as (a) except for salinity. (c) Same as (a) except for density (σ_θ).

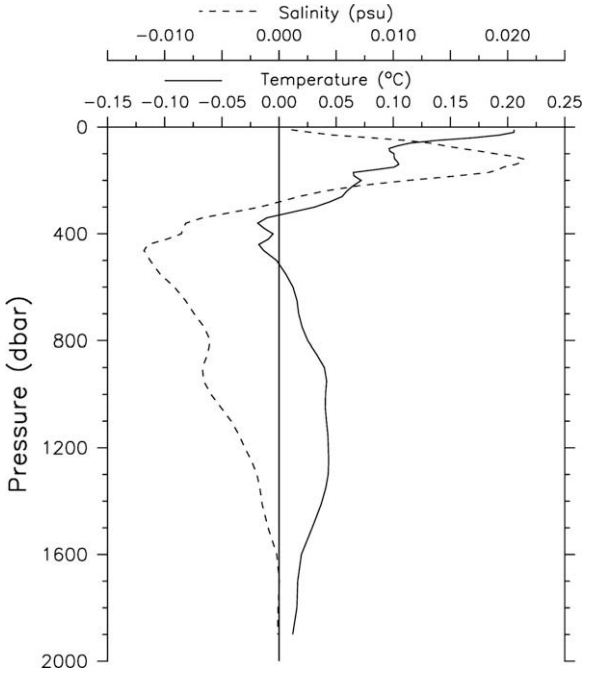

Fig. 3.3. Global average of temperature (solid line) and salinity (dashed) difference versus depth, Argo 5-year mean minus WOA01.

To investigate the causality of temperature and salinity changes, it is useful to separate changes due to vertical displacement of isopleths from those due to changes in the T/S relation. Fig. 3.4 shows zonal averages of Argo salinity and Argo-minus-WOA01 salinity differences on potential density surfaces. The upper 200 dbar is excluded to focus on the subsurface variability. The north/south asymmetry is seen clearly, with the southern freshening being pronounced in the density range from σ_θ equals 26.7–27.3 including Sub-Polar Mode Water and Antarctic Intermediate Water. Shallower densities around σ_θ equals 25.8 show the salinity increase in the evaporative regions. As noted by Bindoff and McDougall (1994), changes in temperature or salinity on density surfaces can be due either to changes in air–sea heat flux or freshwater flux, and additional analysis is needed to separate these causes.

Finally, we provide temporal context for the Argo-minus-WOA01 differences using the pentadal temperature and salinity anomalies for the World Ocean provided by Levitus et al. (2005a) together with mean fields. Again we have converted the Levitus et al. (2005a) depth coordinate to pressure and subsampled in latitude and longitude to match the area included in the Argo climatology. The area-averaged and pressure-averaged (0–2000 dbar) temperature time-series from Levitus et al. (2005a) and from Argo are shown in Fig. 3.5a, with the area-averaged anomaly as a function of pressure shown in Fig. 3.5b. For both Argo and WOA, anomalies are relative to the WOA mean field. The Levitus et al. (2005a) pentadal time-series ends in 1996, so there is a gap between it and

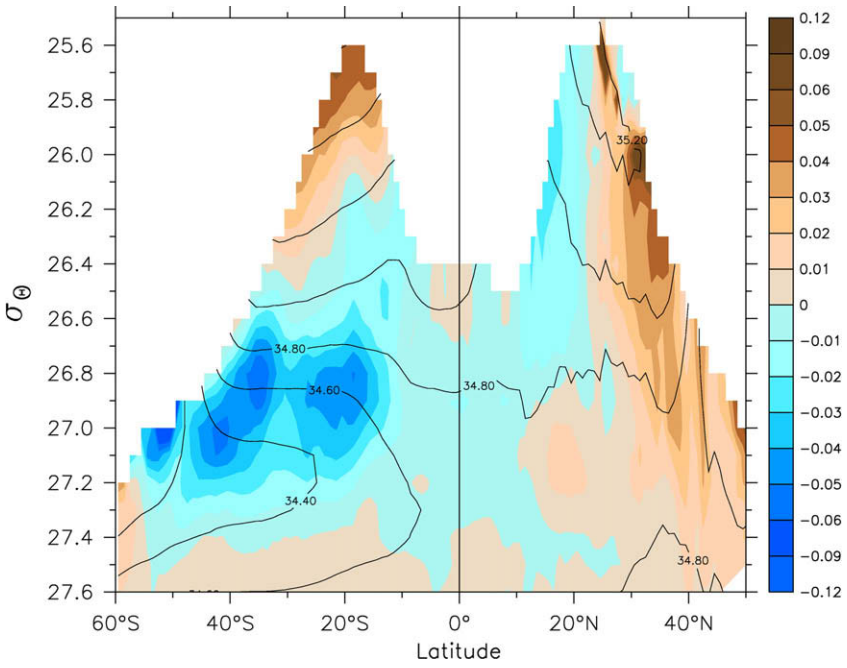

Fig. 3.4. Zonal average of salinity on density (σ_θ) surfaces from the Argo 5-year mean (contours) and Argo-minus-WOA01 difference (color shading).

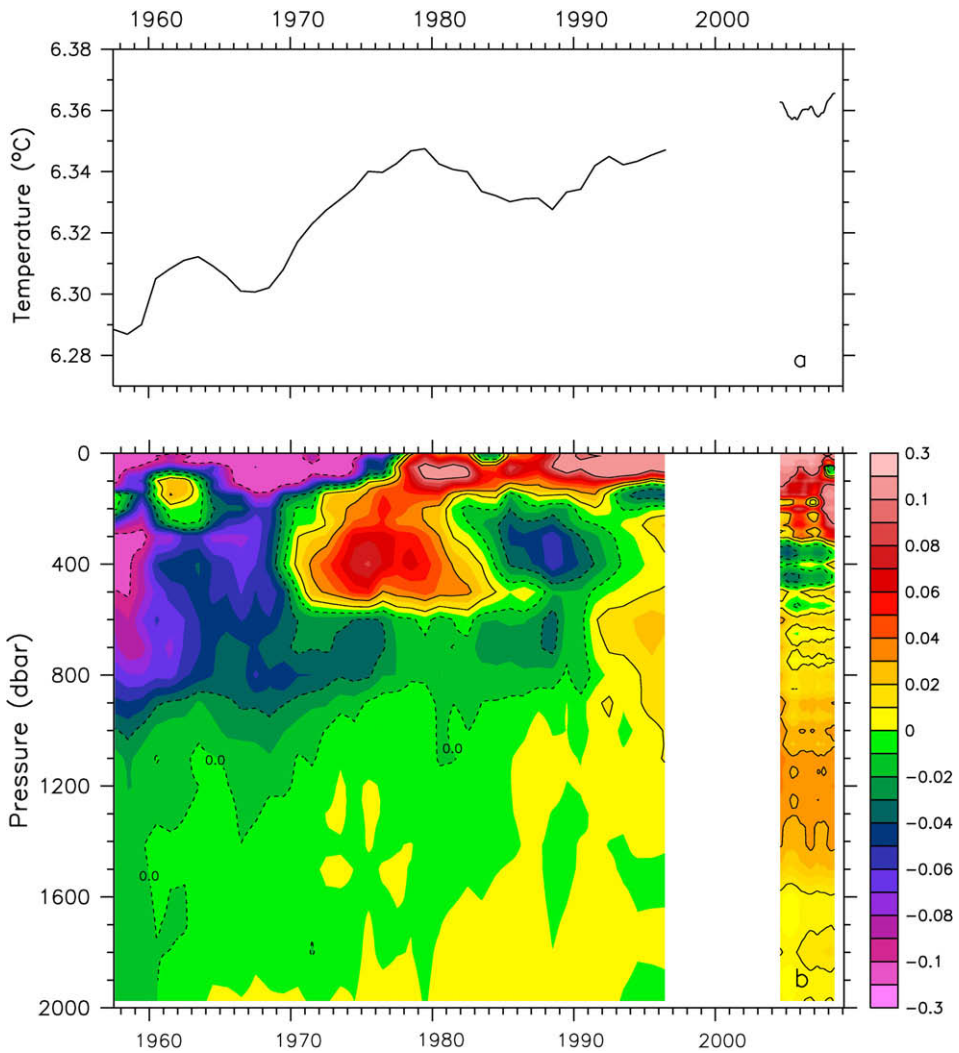

Fig. 3.5. (a) Time-series of temperature averaged globally and over 0–2000 dbar and (b) globally versus pressure from Levitus et al. (2005a) for the period 1957–1996 and from Argo for the period 2004–2008. The Levitus et al. (2005a) data are a 5-year running mean; the Argo data are a 1-year running mean.

the beginning of global Argo coverage. Much of the decadal variability in the Levitus et al. (2005a) time-series in the upper 700 dbar (Fig. 3.5, lower panel) has been attributed by Wijffels et al. (2008) to time-variations in the fall-rate of XBT probes. After correction for fall-rate variations, Wijffels et al. (2008) found a slightly greater long-term trend and reduced decadal variability. The global mean temperature, 0–2000 m from Argo is about 0.07 °C warmer than the WOA estimate 50 years earlier, equivalent to a warming rate of about 0.3 W/m^2. Domingues et al. (2008) applied fall-rate corrections to the historical XBT dataset and estimated the 0–700 m warming rate to be 0.35 ± 0.08 W/m^2 for the period 1961–2003.

3.2. Steric height and ocean circulation

Fig. 3.6a shows the mean steric height of the sea surface relative to 2000 dbar (0/2000) from the Argo climatology. Three subsurface levels, 200, 500, and 1000/2000 dbar are shown in Fig. 3.6c, d, and f. The steric height difference, Argo-minus-WOA01, for the sea surface and the 500 dbar level, is also shown (Fig. 3.6b and e).

The varying depth penetration of the five subtropical gyre interiors is evident in these figures, with the North Pacific interior gyre circulation being the strongest of the five at the sea surface and 200 dbar, while the South Pacific and South Indian gyres have the strongest interior circulations at 1000 dbar. At the 500 and 1000 dbar levels the "Tasman leakage" connection south of Australia between the subtropical South Pacific and Indian gyres (Speich et al., 2002; Ridgway and Dunn, 2007) is seen clearly. Roemmich et al. (2007) noted that the strength of the South Pacific gyre was increased in Argo compared to hydrographic and altimetric data from the early 1990s. A similar increase in all three southern gyres is suggested by Fig. 3.6 in the coincidence of the maximum steric height gain at 500 dbar (Fig. 3.6e) with the latitude of the gyre centers at that depth (Fig. 3.6d). Indeed, that increase is a noticeable circulation difference between Argo steric heights (Fig. 3.6) and previous basin-scale analyses such as Reid (1986) for the South Pacific and Reid (2003) for the Indian Ocean.

Gille (2008) interpreted the multi-decadal change as a southward shift of the Antarctic Circumpolar Current. The location of maxima in sea surface steric height increase (Figs. 3.6b and 3.7), coinciding with maxima in the meridional gradients of steric height (Fig. 3.6a) is consistent with that interpretation. However, Fig. 3.1c suggests that there is downward as well as southward displacement of isopycnals. At the latitude where σ_θ isopleths from 27.0 to 27.6 are deepest, around 40°S, the decreases in density can only be interpreted as deepening of the isopycnals, not as meridional displacements. This can be seen in a vertically inte-

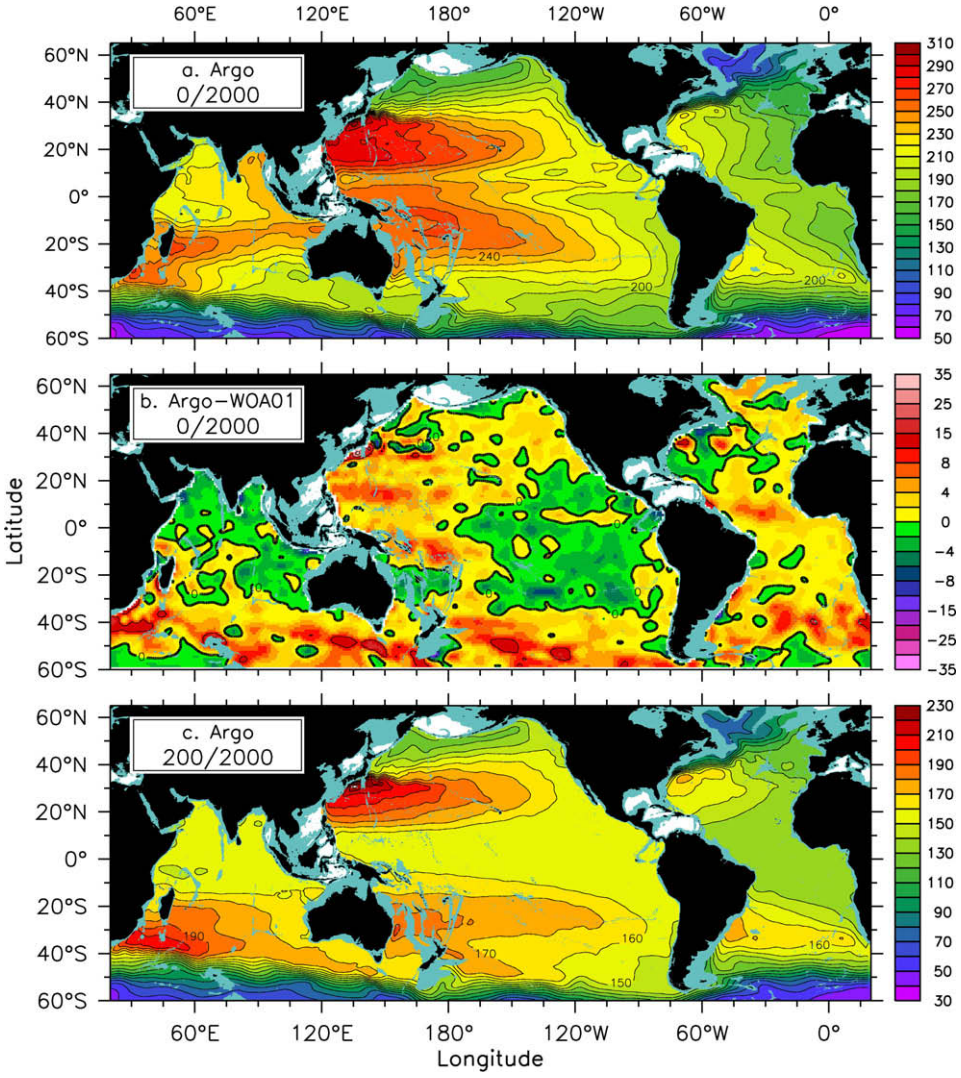

Fig. 3.6. (a) Steric height (dyn cm) of the sea surface relative to 2000 dbar from the 5-year Argo mean. (b) Steric height (0/2000 dbar) difference Argo-minus-WOA01. (c) Same as (a) except for 200/2000 dbar. (d) Same as (a) except for 500/2000 dbar. (e) Same as (b) except for 500/2000 dbar. (f) Same as (a) except for 1000/2000 dbar.

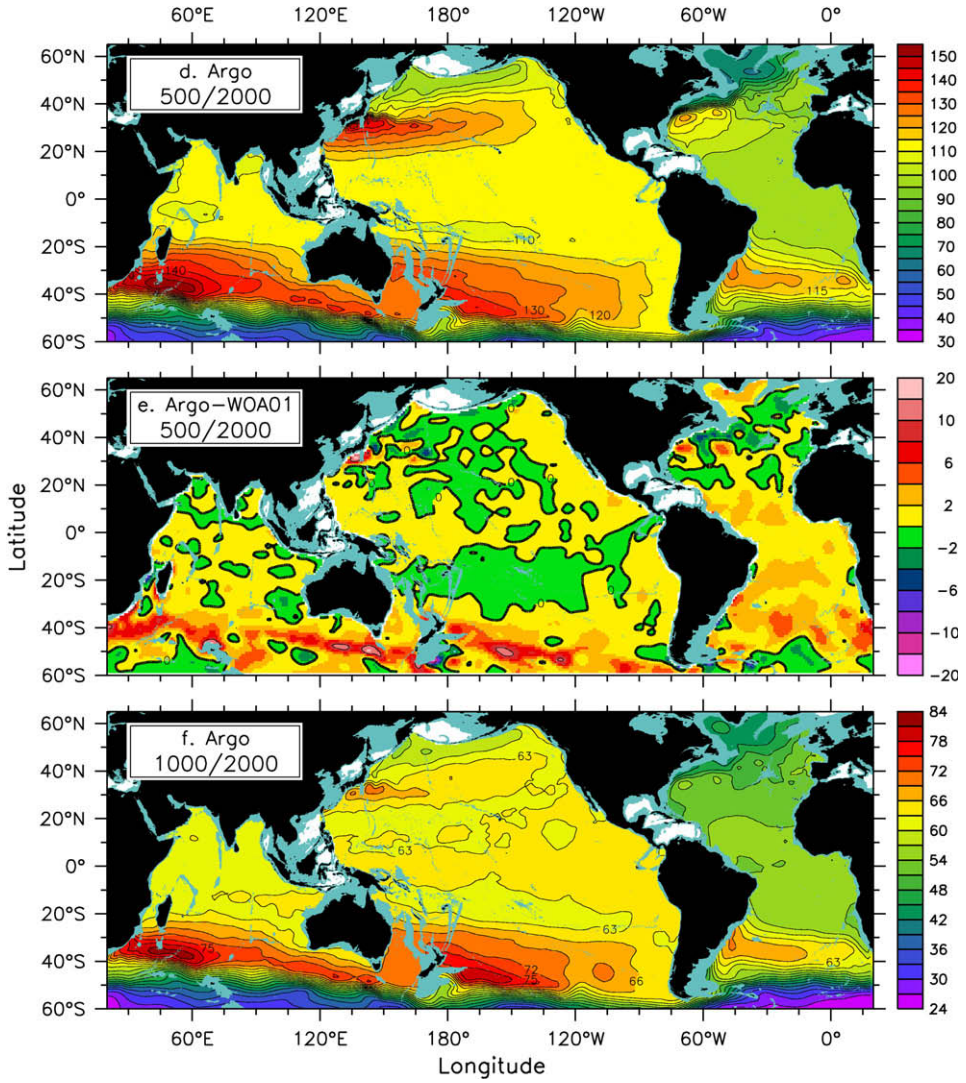

Fig. 3.6. (*continued*)

grated sense in Fig. 3.7. At the latitude near 35°S of the steric height maximum marking the deep gyre center, the Argo-minus-WOCE steric height increase can only be interpreted as deepening of isopycnals.

The zonal averages of the steric height of the sea surface, 200, 500, and 1000 dbar, relative to 2000 dbar, are shown in Fig. 3.7. The tendency of the southern subtropical gyres to extend deeper in the water column is seen at the 1000 dbar, and even the 500 dbar level, where the southern high is more prominent than the northern one. The zonal averages of steric height difference, Argo-minus-WOA, show the southern height increase extending deep into the water column over latitudes from 30°S to 60°S.

As noted earlier, the warming in the northern North Atlantic is partly density-compensated due to a salinity increase. Therefore the steric height changes seen there are more limited in north–south extent. There are also steric height increases in Argo relative to WOA01 in the tropical Atlantic and the western Pacific (Fig. 3.6b), particularly the Kuroshio region. The dominance of the Southern Ocean signal in steric height difference is seen in large-area averages. South of 30°S, the steric height of the sea surface (0/2000 dbar) is higher in the Argo climatology by an average of 3.5 dyn cm while over the rest of the ocean north of 30°S the average is only 0.7 dyn cm.

3.3. Sampling errors

Argo is a sparse array, and its capability to estimate mean fields and low frequency variability depends on averages over energetic noise due to eddies, fronts, and other unresolved variability. Systematic errors in the mean field, as well as in the variability, can be introduced by irregularities in float deployment patterns, such as the tendency for fewer floats to be deployed south of 50°S in the Southern Ocean, by convergences of floats caused by drift on the sea surface or at depth, or by analysis methods.

A variety of estimates can be made of Argo's effectiveness in view of both the errors caused by the array's overall sparseness and those due to its unevenness.

(1) Formal error estimates result from the optimal interpolation. As noted by Davis (1998), the error estimates are more sensitive to details of the covariance function than are the maps themselves.
(2) Error estimates can be made by using satellite altimetric height as a proxy for steric height. On large spatial and long temporal scales, variations in the height of the sea surface measured by satellite altimetry are dominated by density fluctuations (e.g. White and Tai, 1995; Gilson et al., 1998).

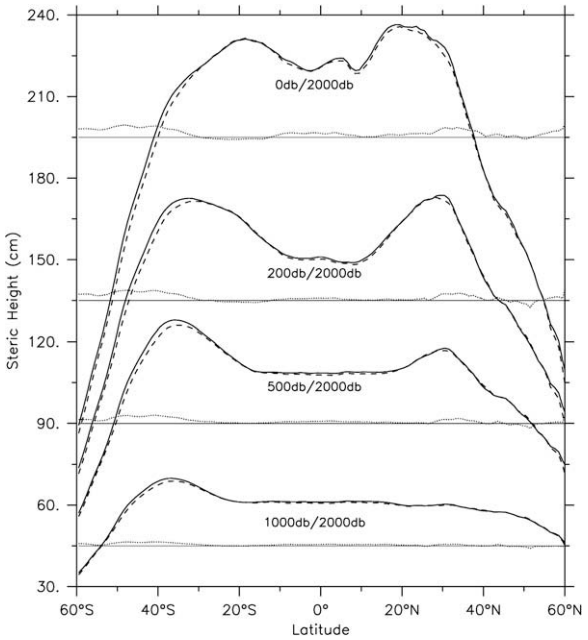

Fig. 3.7. Zonal average of steric height of the sea surface, 200, 500, and 1000 dbar surfaces relative to 2000 dbar for Argo (solid lines), WOA01 (dashed), and for the Argo-minus-WOA01 difference (thin dotted lines, with origins offset).

Altimetric height, and especially the multi-altimeter product used here (Ducet et al., 2000), has higher intrinsic resolution than Argo and thus serves as a useful proxy for steric height in estimating Argo sampling error. Limitations are (i) sea surface height also contains variability due to mass and to abyssal-ocean density changes that are not in Argo data and (ii) altimetric height does not resolve mesoscale variability in the across-track direction.

(3) The Argo dataset can be divided into subsets that are mapped separately and compared to one another. For increased statistical independence between groups, the subsets here will include all profiles from a given float, rather than selecting by profile.

(4) Argo can be compared to related but independent datasets. An example is provided by Hadfield et al. (2007), comparing an interpolated Argo dataset in the Atlantic with a hydrographic transect along 36°N. A comparison is made below of Argo's near-surface temperature with the NOAA Optimal Interpolation SST product (NOAA OI SST, Reynolds et al., 2002).

First, the impact of Argo sampling errors on the mean sea surface steric height field (Fig. 3.6a) is considered. Since the Argo era is being compared with the WOA01 climatology, a question is whether the differences between the estimated Argo mean and WOA01, shown in Fig. 3.6, are larger than the Argo sampling errors. To address this question, the 2004–2007 altimetric height mean was subtracted from the gridded AVISO altimetric height field (Ducet et al., 2000) and replaced by the annual mean steric height (0/2000 dbar) from WOA01. This combination of the WOA01 mean plus the altimetric height anomaly was then subsampled at the space and time location of each Argo profile. The subsampled field was subjected to the same two-step fitting and objective analysis procedure that was described for Argo data in Section 2. Finally, this subsampled and mapped 48-month average was compared to WOA01. This error estimate is dependent on the mean field chosen for the experiment, here WOA01, so it is not an estimate of the absolute error in the Argo mean. However, other similarly realistic mean fields will produce similar error estimates.

Fig. 3.8 shows a map of the error in the mean estimated in this way (Fig. 3.8a) as well as zonal averages of the Argo-minus-WOA01 steric height difference (0/2000 dbar, dotted line from Fig. 3.7) and of the error in the mean (Fig. 3.8b). The sampling error is substantial in the Southern Ocean, but is much less in the zonal average than the overall steric height increase between 30°S and 60°S. In general, strong property gradients in the mean field are under-estimated by the sparsely sampled data. This can be seen in reversals in sign of the estimated error between 4°N and 10°N in the North Equatorial Current, in the separated western boundary currents and in the Antarctic Circumpolar Current. In each case sign reversals in the error map (Fig. 3.8a) indicate that the fitting and mapping procedure underestimates the meridional gradient in steric height. Globally, the RMS of the estimated error in mean steric height, for $3^\circ \times 3^\circ$ smoothing, is 1.7 cm, and only 1.3 cm between 30°S and 30°N. This estimate of sampling error applies only to the Argo mean, and the corresponding sampling error in WOA01 may be larger and is more difficult to quantify.

A primary objective of Argo is estimation of seasonal-to-interannual variability on large-spatial scales. Again, altimetric height can be used as a proxy, but this time to estimate the errors in large-scale steric height variability. First the $1/3^\circ \times 1/3^\circ \times$ weekly gridded AVISO altimetric height anomalies, with the 2004–2007 altimetric height mean removed, were smoothed with a running

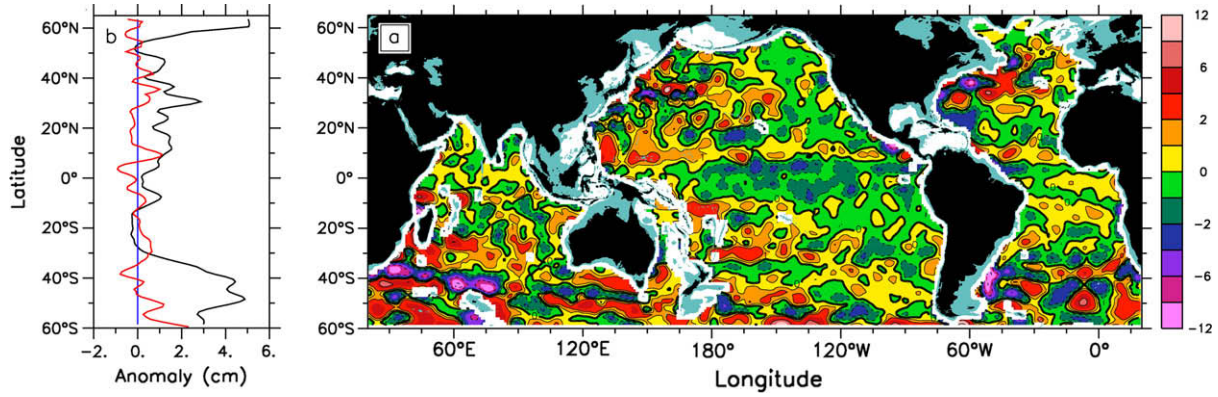

Fig. 3.8. Argo sampling error's impact on mean sea surface height ((a) spatial map, (b) zonally averaged, cm), based on adding altimetric height variations (subsampled at Argo profile locations versus not subsampled) to the WOA01 mean steric height (0/2000 dbar). For comparison to the error estimate (red line), zonally averaged difference of Argo-minus-WOA01 steric height (0/2000 dbar) is also shown (black line).

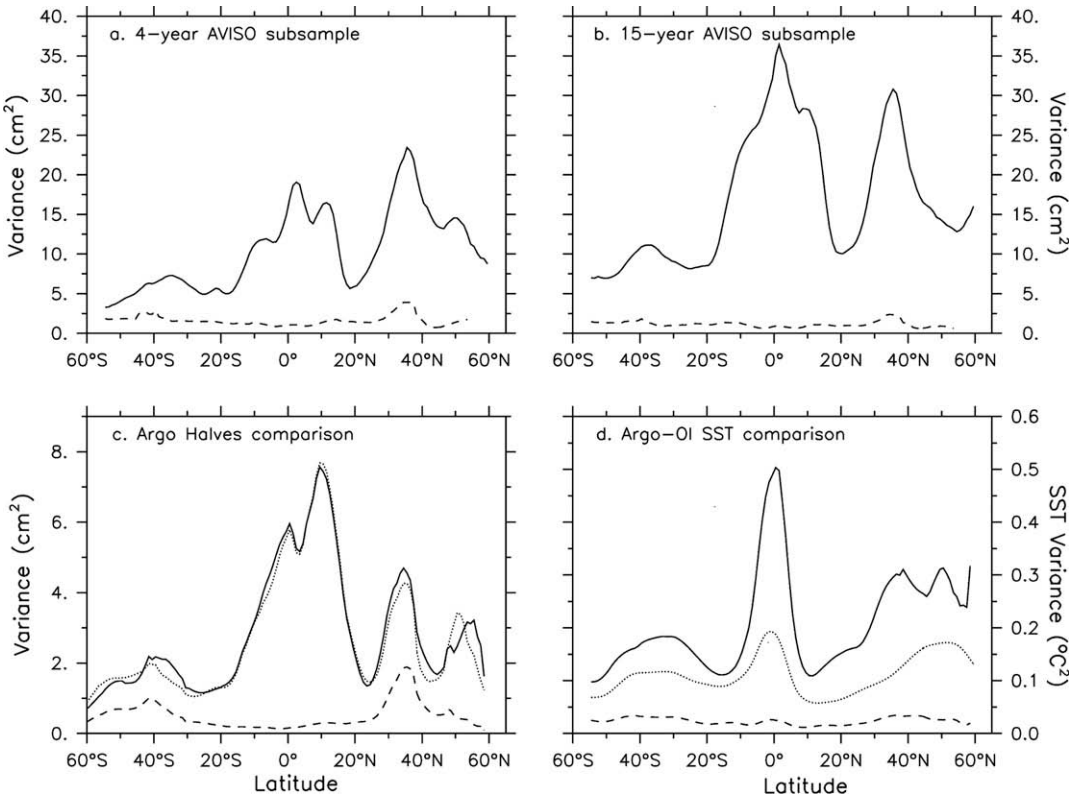

Fig. 3.9. (a) Zonally averaged variance (cm^2) of large-scale ($10^\circ \times 10^\circ \times 3$ month) altimetric height variability for 2004–2007 (solid line). Argo sampling error, 2004–2007 (dashed), is estimated from the difference between the complete altimetric height dataset and that subsampled at Argo profile locations. (b) Same except using 1993–2007 altimetric height variability, and error based on sub-sampling that period each year at the location and year-day of Argo profiles from 2008. (c) Zonally averaged variance (cm^2) of large-scale Argo steric height variability for each of two halves of the 2004–2008 Argo dataset (solid and dotted lines); zonally averaged variance of large-scale steric height difference between either half and the sample mean (dashed). (d) Zonally averaged variance ($°C^2$) of the large-scale smoothed NOAA OI SST dataset, for years 1993–2007 (solid) and 2004–2008 (dotted). The dashed line is the variance of the large-scale difference between Argo and NOAA OI SST, 2004–2008.

mean over $10^\circ \times 10^\circ \times 3$ month scales. For the smoothed data, the variance of temporal anomalies was then zonally averaged (Fig. 3.9a, solid line) to show the latitude dependence of the large-scale signal. Next, the unsmoothed AVISO data, with the 2004–2007 mean removed, were subsampled at the location and time of each Argo profile. The subsampled dataset was then objectively interpolated using the same procedures as the Argo data, and the mapped fields were smoothed over the $10^\circ \times 10^\circ \times 3$ month scales. At full Argo resolution, a $10^\circ \times 10^\circ \times 3$ month region contains about 100 profiles. The large-scale Argo sampling error was then estimated as the difference between the full and subsampled, smoothed altimetric height (Fig. 3.9a, dashed line). The large-scale signal variance changes with latitude from about 5 to 20 cm^2, while the error varies between about 1 and 3 cm^2. The ratio of signal to error variance is about 3 in the Southern Ocean but more than 10 in the equatorial zone.

Fig. 3.9b shows a further experiment in which the 15-year AVISO dataset, 1993–2007, is subsampled each year at the location and year-day of the 2008 Argo profiles. The subsampled dataset is re-mapped, smoothed, and again compared to the full dataset. Compared to Fig. 3.9a, the noise is reduced in Fig. 3.9b since Argo sampling during 2008 was more complete than during 2004–2007. The signal is increased in the 15-year experiment as more interannual and decadal variability appears in the lengthened time-series. These estimates of noise-to-signal ratio from the altimetric height subsampling experiments are lower bounds to the extent that the AVISO altimetric height fields do not contain all of the small-scale variability of the point-wise Argo profile data.

A more direct estimate of signal and noise is made by randomly sorting the Argo array into two separate groups of floats. Each of these groups is used to estimate the 60-month time-series of temperature and salinity anomaly fields using the same optimal interpolation procedure. Steric height (0/2000 dbar) is calculated and smoothed, again with a $10^\circ \times 10^\circ \times 3$-month running mean. Fig. 3.9c shows the zonal mean of steric height variance for the two groups, plus error variance estimated over 60 months from the difference between either of the two groups and the two-group mean. The signal variance is reduced relative to the 4-year altimetric height dataset because (i) the optimal interpolation of the sparser Argo groups systematically underestimates the anomaly fields and (ii) the steric height (0/2000 dbar) fields do not include deep steric or mass-related contributions to sea surface height. As in the altimetric height experiments, the error in large-scale steric height is seen to be 1 cm^2 or less at most latitudes, with a minimum at the equator and maxima near 40°N and 40°S. The noise-to-signal ratio is high, about 0.5, south of 30°S, highlighting a need for more floats in that important region.

A final global estimate of signal and noise is made by comparing near-surface Argo temperature anomalies with the NOAA OI SST (Reynolds et al., 2002) product. Argo data are not presently used in generating the NOAA OI fields, so the two estimates are completely independent. The shallowest Argo data are typically at about 5 m depth. The NOAA OI product uses satellite data adjusted for consistency with drifter measurements of temperature at about 0.5 m depth, so temperature stratification could contribute to systematic differences between the Argo and NOAA OI SST estimates. Fig. 3.9d shows the zonal mean variance of smoothed NOAA OI SST anomalies for both a 5-year, 2004–2008, and a 15-year, 1993–2007, time-series. Again one can see the increase in signal variance as the time-series is lengthened. The error variance is estimated

from the 60 monthly differences, again smoothed to 10° × 10° × 3 months, of Argo-minus-NOAA OI SST for the period 2004–2008. This difference is an upper bound on the error attributable to Argo mapping errors, since the NOAA OI product also has some large-scale error.

The diverse error estimates shown in Fig. 3.9 have a number of similarities. They demonstrate that Argo does a good job of estimating large-scale anomaly fields in the tropics, where interannual signals are large and steric height errors are less than 1 cm. The errors grow to maxima at the latitudes of the separated western boundary currents, and more floats are needed there to lower the noise-to-signal ratio, especially in the large southern hemisphere oceans.

4. The 2004–2008 annual cycle

For estimation of the annual cycle, the 5-year Argo record was averaged for each month, i.e. five Januarys, etc. The smoothed fields and analyzed quantities such as surface layer heat gain were calculated from the monthly time-series prior to the 5-year averaging.

4.1. Temperature

The difference between zonally averaged March and September temperature (Fig. 4.1) reveals interesting hemispheric asymmetries. Most strikingly, the northern oceans show a maximum seasonal temperature change at the sea surface of 9.4 °C at 42°N, while the corresponding southern maximum is only 5.3 °C at 35°S. In both hemispheres at middle latitudes this seasonal contrast drops to about 3 °C at 50 m; hence the northern oceans have a substantially more stratified surface layer in summer (Fig. 4.2) than the southern ones. These findings are similar to historical datasets (WOA01 and Levitus and Antonov, 1997). The pronounced asymmetry in seasonal temperature change may include contributions from air–sea flux and from ocean heat advection at the latitudes of the separated western boundary currents. Examination of the NOC air–sea flux climatology (Version 1.1, Josey et al., 1998) shows that the zonal average of latent heat flux at 42°N has annual amplitude of 40 W/m^2, versus 15 W/m^2 at 35°S. The subsurface maxima in temperature variability in the tropics seen in Fig. 4.1 are dynamical signals, discussed below.

4.2. Sea-surface temperature

Fig. 4.3 compares the annual cycle in zonally averaged Argo near-sea surface temperature (SST) with that of the NOAA OI (Reynolds et al., 2002) monthly averaged SST product. The latter dataset was masked to the same spatial grid as Argo, removing shallow regions and marginal seas, and averaged over the same 5-year period from 2004 to 2008. The two panels of Fig. 4.3 are strikingly similar in pattern and magnitude. Compared to the values noted above for the March-minus-September SST changes for Argo, the NOAA OI product shows similar seasonal differences, 9.5 °C at 42°N and 5.4 °C at 35°S. When the Argo and NOAA OI SST grids are further averaged to hemispheric and global means (Fig. 4.4), the monthly mean differences are small, about 0.02 °C for global and 0.04 °C for hemispheric averages.

We also compared Argo near-surface temperatures with nearby surface drifter measurements of SST. About 27,000 Argo/drifter pairs were found within 60 km and 10 days of one another during 2004–2008. Differences due to stratification were seen only in small subsets of daytime, low-wind (<3 m/s) pairs of measurements. Differences averaged over all conditions were small (∼.01°) at all temperatures. The good agreement between Argo and the NOAA OI SST product, shown in Figs. 3.9, 4.3, and 4.4, is owing to the similarity between Argo and drifter temperature measurements and to Argo's good spatial coverage enabling accurate interpolation of large-scale fields.

4.3. Heat gain

The monthly heat gain by the ocean's surface layer was calculated from the Argo climatology by averaging temperature over a depth range that includes all locally outcropping waters. The calculation was similar to that described by Moisan and Niiler (1998), but here using density instead of temperature to locate the base of the surface layer:

$$\text{heat gain} = \rho c_p \left(\langle h \rangle \frac{\partial < T_a >}{\partial t} \right)$$

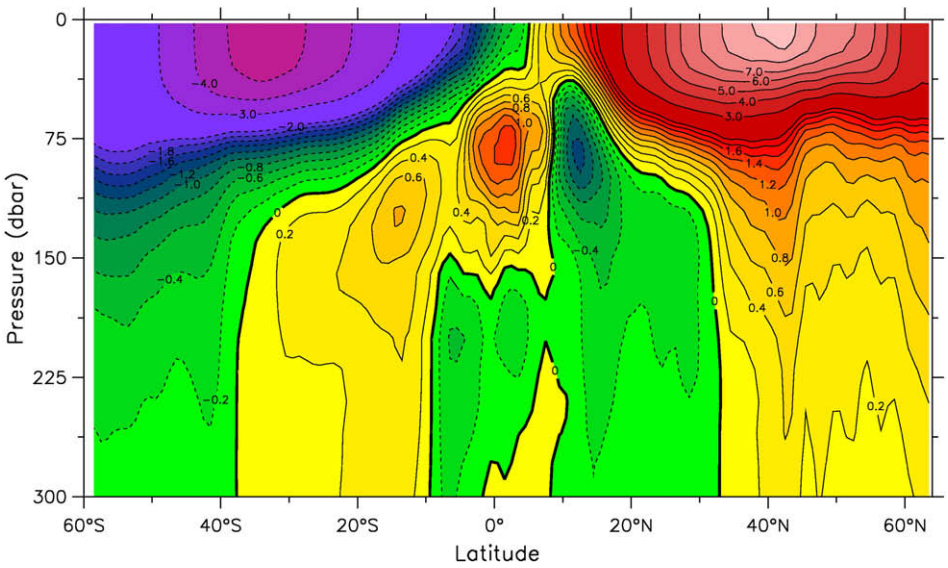

Fig. 4.1. Zonally averaged September-minus-March temperature difference (°C) versus pressure for the Argo 5-year mean.

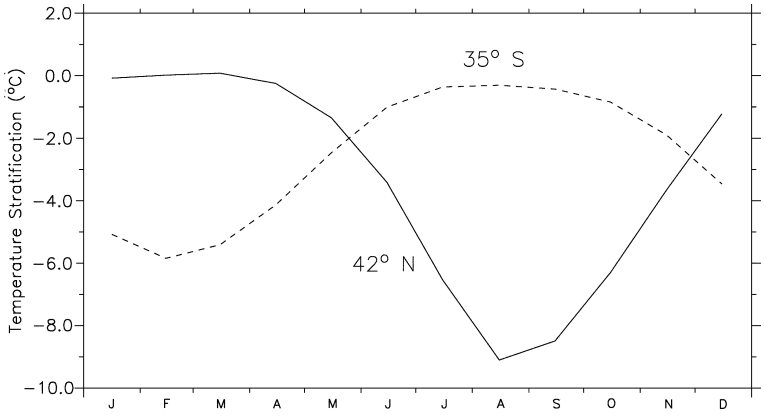

Fig. 4.2. Annual cycle of zonally averaged temperature stratification in the upper 100 dbar ($T_{100} - T_0$, °C) at 42°N (solid line) and 35°S (dashed).

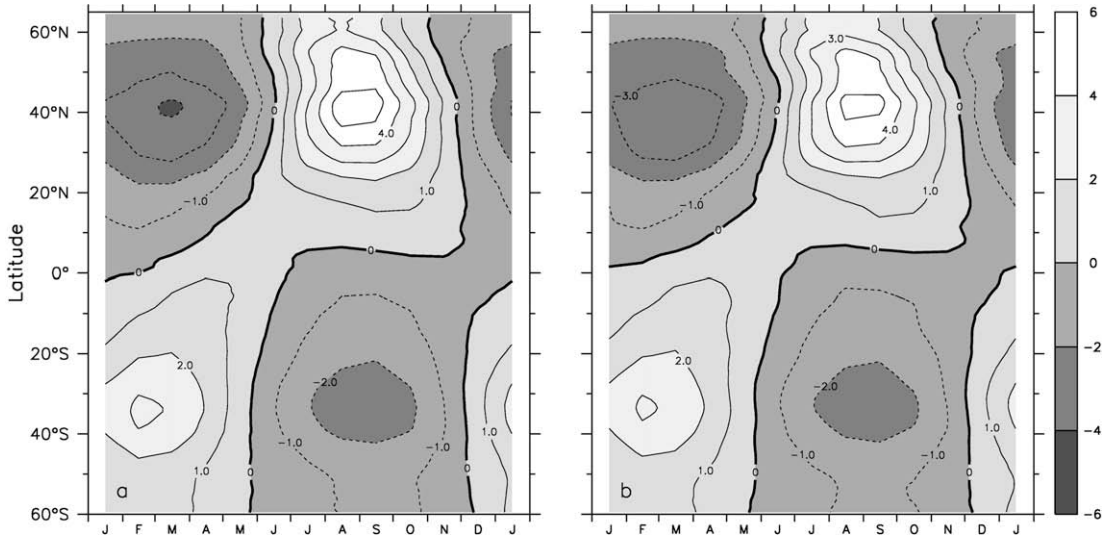

Fig. 4.3. Annual cycle of zonally averaged near-sea surface temperature (°C) anomaly, 2004–2008, from Argo (a) and from the NOAA OI SST product (Reynolds et al., 2002, (b)).

where $\langle h \rangle$ is the monthly mean depth of a "nearly outcropping" density surface, defined by the densest isopycnal seen at the sea surface at a given location over the 5-year period, plus 0.05 (σ_θ). $\langle T_a \rangle$ is the monthly and vertically averaged temperature above that "nearly outcropping" isopycnal. The choice of the base of the surface layer is an imperfect tradeoff, intended to minimize both adiabatic changes in heat content due to vertical advection of deep isotherms and downward heat loss from the surface layer due to vertical mixing.

The surface layer heat gain defined as above was compared to air–sea heat flux from the National Oceanography Centre (NOC) 1.1 climatology (Josey et al., 1998). The hemispheric and global averages of the annual cycle of surface layer heat gain are shown in Fig. 4.5 together with the NOC 1.1 product. The annual mean was removed from the air–sea flux, and that dataset was masked so that its spatial grid matched that of the Argo grid (60°S to 65°N, with marginal seas omitted). The two datasets are in reasonable agreement on these planetary scales, with amplitude greater in the Argo dataset by about 5 W/m^2. This difference, and the small phase difference, could be attributed to systematic errors in either estimate or to interannual variability, with the Argo data representing the mean for 2004–2008, and the NOC dataset being compiled from marine meteorological reports during 1980–1993. Another possible contributor to the hemispheric differences is annual variability in cross-equatorial ocean heat transport. The phase difference decreases if the surface layer heat gain is integrated to a deeper isopycnal, consistent with downward diffusion of heat at the base of the layer.

In Fig. 4.6, zonally averaged monthly heat gain from Argo is compared to zonally averaged air–sea heat flux from the NOC climatology, with the annual mean removed from the latter. The annual patterns of ocean heat gain and air–sea flux are very similar, consistent with the interior ocean scaling argument presented by Gill and Niiler (1973). However, at middle latitudes in both hemispheres the amplitude of ocean heat gain exceeds that of air–sea flux – by about 50 W/m^2 at 40°N and 25 W/m^2 at 40°S. At these latitudes the zonally averaged temperature fields (Fig. 3.1) have strong meridional gradients due to zonal flow in the separated western boundary currents. The Gill and Niiler (1973) interior ocean scaling does not hold in these regions, where seasonal advection may be significant. Clear evidence that these discrepancies occur in the western boundary currents was seen in monthly anomaly maps of ocean heat gain minus air–sea heat flux (not shown). Further support for this explanation was found in the salinity field discussed below.

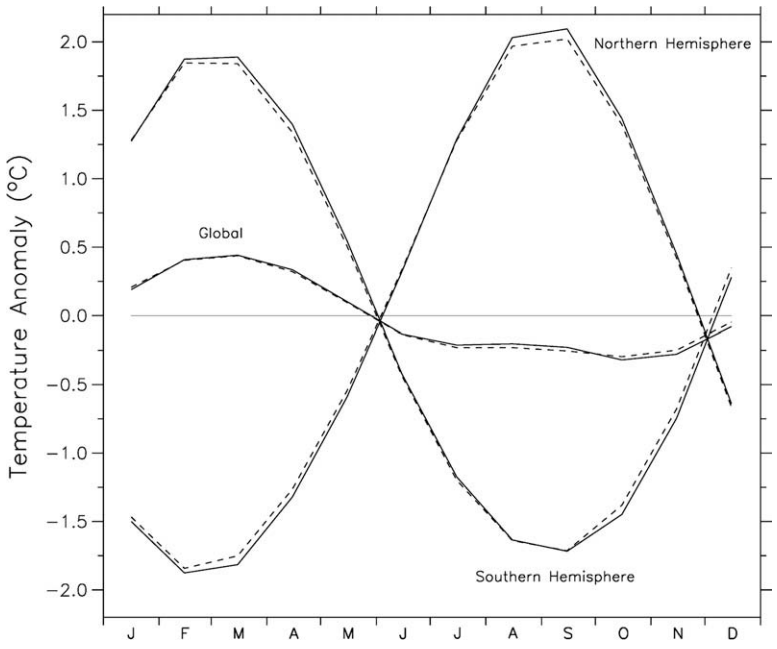

Fig. 4.4. Annual cycle in the area-averaged NOAA OI SST product (dashed) and Argo near-surface temperature (solid) for the northern hemisphere, southern hemisphere, and global ocean, 2004–2008.

4.4. Salinity, freshwater content, and sea-surface salinity

The difference between zonally averaged March and September upper-ocean salinity is shown in Fig. 4.7. This is analogous to the seasonal temperature difference of Fig. 4.1, but with salinity contours from the Argo 5-year mean overlain. Several things are evident in this figure. First, the low latitude northern and southern atmospheric convergence zones are seen as out-of-phase maxima in the seasonal salinity signals at the sea surface. The maximum in salinity difference at about 8°N corresponds well with the minimum in sea-surface salinity (contours). While the seasonality is equivalent in the two hemispheres, the mean salinity is much lower below the northern Inter-Tropical Convergence Zone (ITCZ) due to the stronger zonally averaged annual mean precipitation there than in the south, where the South Pacific Convergence Zone dominates the zonal average.

Second, the net evaporative regions with high mean salinity at about 25°N and 25°S have minima in seasonality. The seasonal contrasts increase again at high latitudes where mean rainfall is high and mean salinity is low. Of interest are the seasonal signals at about 100 dbar at 40°N and to a lesser extent 40°S. The subsurface phase reversal at 40°N relative to the sur-

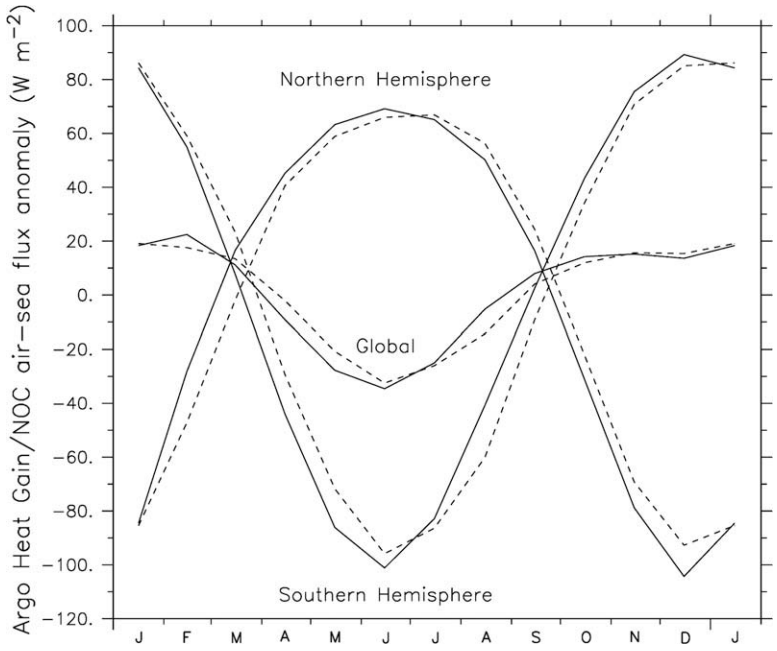

Fig. 4.5. Annual cycle in area-averaged ocean heat storage from Argo (W/m^2, solid lines, see text for details) compared to air–sea heat flux anomaly from the NOC 1.1 climatology (dashed, Josey et al., 1998), for the northern hemisphere, southern hemisphere, and global ocean.

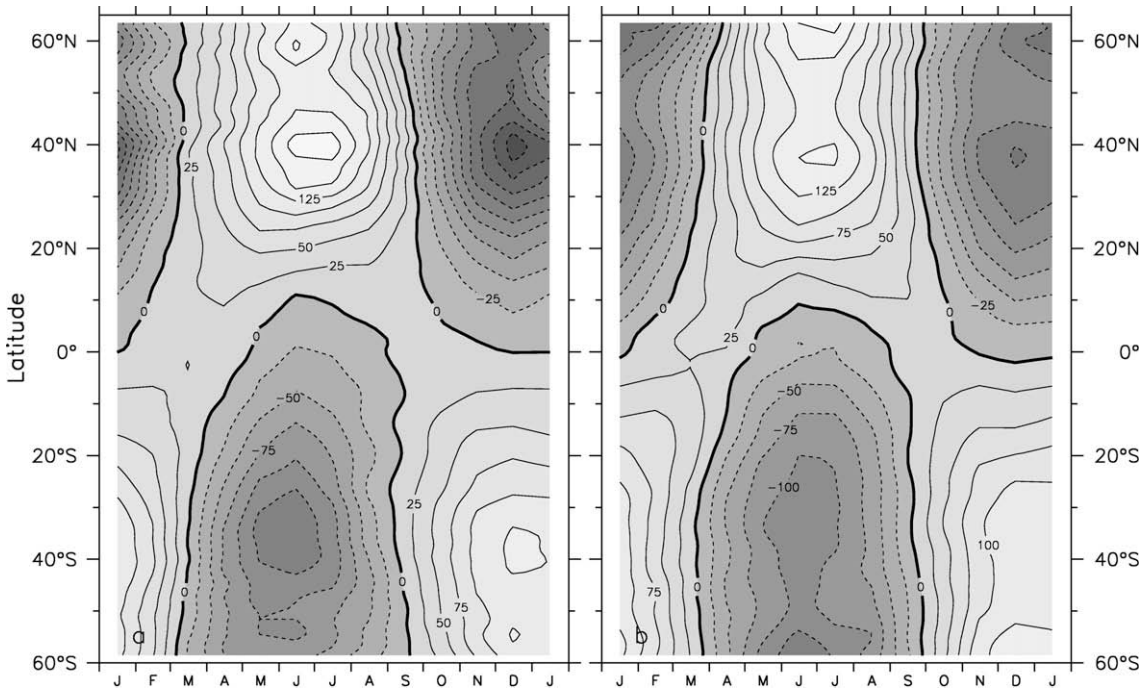

Fig. 4.6. Annual cycle in zonally averaged ocean heat storage from Argo (W/m^2, a) compared to air–sea heat flux anomaly from the NOC 1.1 climatology (b).

face layer at that location, also seen in historical data by Levitus (1986), suggests an explanation other than P – E. Instead, these signals are consistent with small meridional displacements of the mean salinity field, as are the seasonal temperature changes at these locations (Fig. 4.1) and with the discrepancy between seasonal ocean heat gain and air–sea heat flux noted above. Future improvement in the comparison between heat and freshwater air–sea exchanges and oceanic storage will require that the ocean's advective component be included, even for seasonal variations.

Finally, just as the annual mean salinity has more meridional structure than the temperature field (Fig. 3.1a and b), so the seasonally varying salinity (Fig. 4.7) is more structured than seasonally varying temperature (Fig. 4.1). This and the likelihood of greater sampling errors in seasonal precipitation estimates than in air–sea heat fluxes makes it more problematic to compare freshwater storage with P – E. In doing so (not shown), we still found reasonable agreement between seasonal freshwater gain in the surface layer and P – E from the NOC climatology in the latitude band of the ITCZ, but less so at other latitudes.

A comparison of the annual cycle in sea-surface salinity (SSS) between Argo and WOA01 is shown in Fig. 4.8. Argo and WOA01 show a similar pattern of annual variability in SSS, but with lower amplitude in Argo, particularly in the northern tropics. This could be due to interannual variability, with Argo representing a 5-year interval, 2004–2008, and WOA01 an earlier and longer one. The tropical Pacific north of 8°S had regular sampling of upper-ocean temperature and salinity during the 1990s by the TAO program

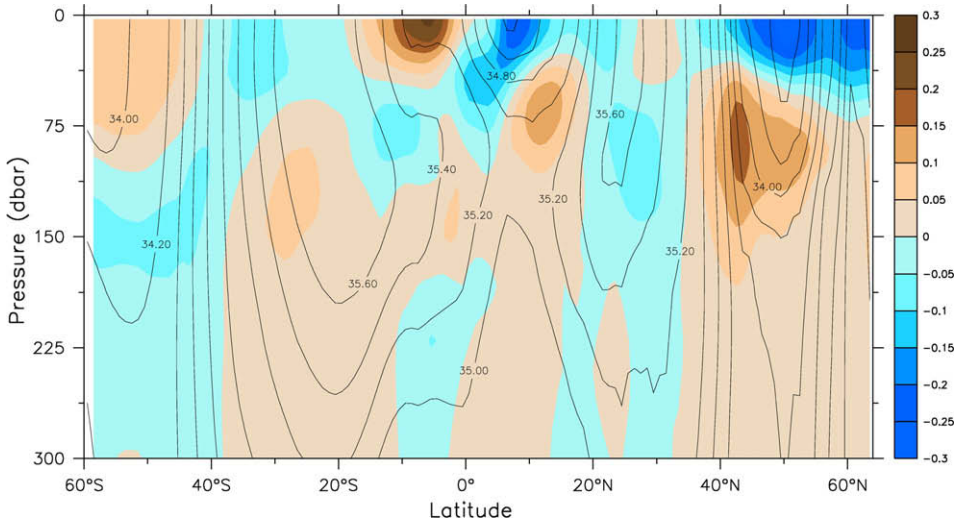

Fig. 4.7. Zonally averaged September-minus-March salinity difference (color shading) versus pressure for the Argo climatology; zonally averaged Argo annual mean salinity (contours).

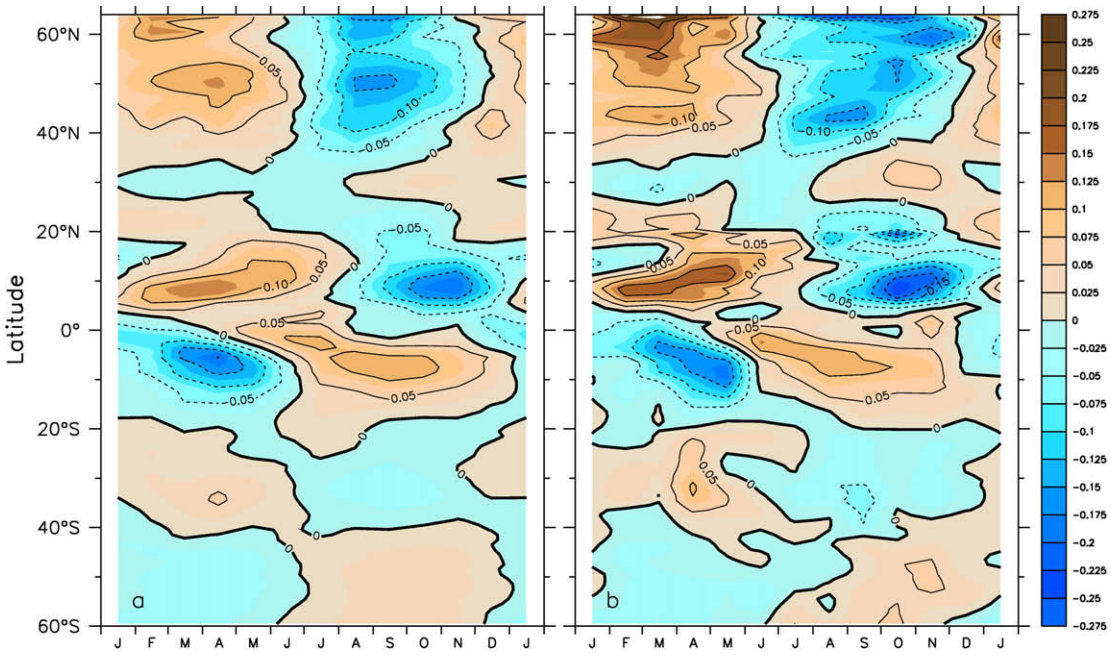

Fig. 4.8. Annual cycle in near-sea-surface salinity anomaly (from the annual mean) from Argo (a) and WOA01 (b).

(e.g. Johnson et al., 2002), so that decade is well represented in the historical dataset.

4.5. Steric height and ocean circulation

The annual cycle of steric height is dominated in most regions by changes in the heat content of the surface layer, with smaller contributions from salinity and from subsurface temperature changes due to ocean dynamics. Fig. 4.9 shows the annual cycle of steric height (0/2000 dbar) for northern and southern hemisphere averages and for the global average (solid lines). Annual means have been removed from each. The southern hemisphere maximum in March at 2.2 cm is lower than the corresponding northern hemisphere value of 2.7 cm in September. However, since the southern hemisphere oceans have much greater area, the phase of the global average follows that of the southern hemisphere, though the amplitude is greatly reduced by the hemispheric cancellation. A similar signal was seen in comparison of steric height from historical data with early years of satellite altimetry by Levitus et al. (1997).

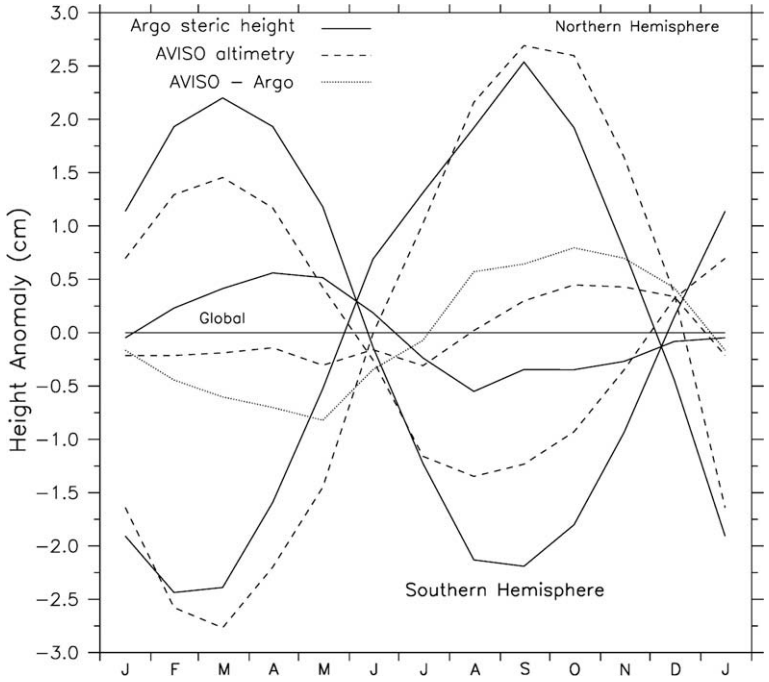

Fig. 4.9. Annual cycle in area-averaged Argo steric height of the sea surface (solid lines, 0/2000 dbar, annual mean removed) compared to altimetric height (dashed, AVISO product) for the northern hemisphere, southern hemisphere and global ocean. The dotted line is the global average of altimetric height minus steric height.

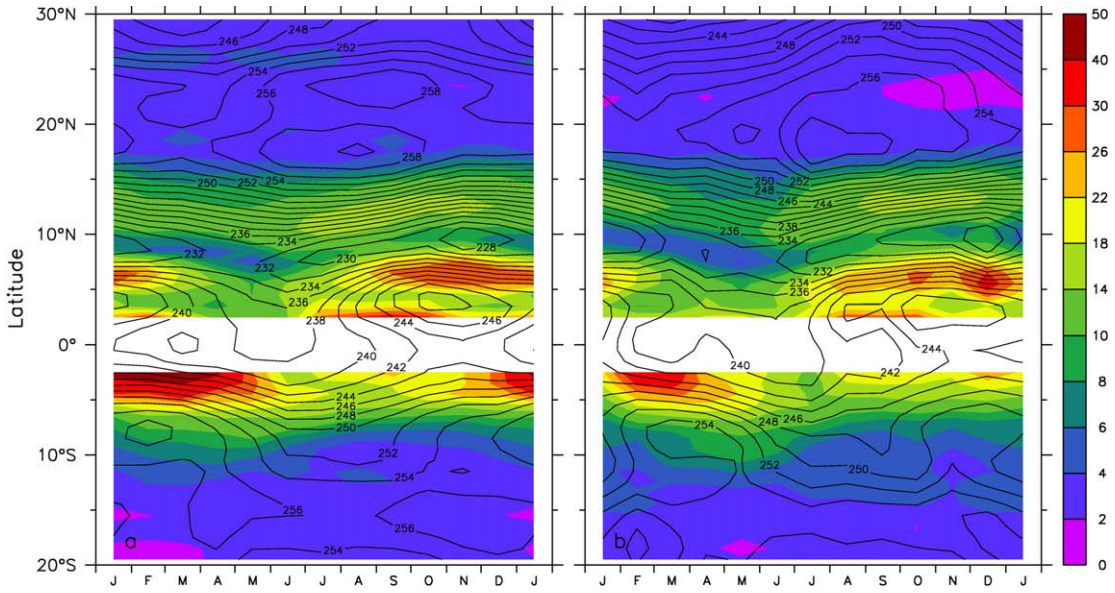

Fig. 4.10. Annual cycle in zonally averaged Central Pacific (160°E–140°W) steric height (0/2000 dbar) from Argo ((a) contours) and from WOA01 ((b) contours). The color shading indicates the corresponding speed of the surface geostrophic flow, $(u^2 + v^2)^{1/2}$, omitting values within 3° of the equator.

Annual sea surface height variability includes the upper ocean steric height contribution plus any annual variability in deep ocean steric height and variability in mass (bottom pressure). Fig. 4.9 shows the annual sea surface height variability from satellite altimetry (Ducet et al., 2000, dashed lines), masked to represent the same northern hemisphere, southern hemisphere, and global regions as the Argo steric height. The averages were calculated for the 2004–2007 period (not all of 2008 is presently available in altimetric height). If we compare the Argo steric height annual cycle with historical data (WOA01) or compare the 2004–2007 altimetric height with the full 1993–2007 altimetric record, the resulting differences due to interannual-to-decadal variability are smaller than the differences between steric height and altimetric height seen in Fig. 4.9. The fact that the southern hemisphere steric annual cycle has greater amplitude than its altimetric height counterpart is interesting, and suggests a reduction in the latter due to inter-hemispheric and sea–land exchanges of mass. The out-of phase relationship between the global averages of steric height and altimetric height has been noted previously, e.g. by Chen et al. (1998), and attributed to seasonal continental storage of water. The global average of altimetric height minus steric height, also shown in Fig. 4.9 (dotted line), is similar to that of Chambers et al. (2004), who analyzed historical steric height data for this purpose, and reported the difference to be similar to mass variability measured by the GRACE satellite mission.

Geostrophic velocity and transport in the tropics has long been known to have substantial seasonal variability (e.g. Wyrtki, 1974). The subsurface maxima in September-minus-March temperature differences, Fig. 4.1, are an expression of this dynamical signal during those months. In Fig. 4.10, the annual cycle in sea surface steric height (0/2000 dbar), zonally averaged in the central Pacific Ocean from 160°E to 140°W is shown for Argo and WOA01. A similar figure is shown by (Wyrtki, 1974, Fig. 3). Fig. 4.10 also shows the speed of the geostrophic flow on the sea surface, averaged over the same longitude range. The Argo and WOA01 patterns of annual variability in tropical Pacific steric height are quite similar. Argo shows less annual variation in the steric trough that marks the northern edge of the North Equatorial Counter Current (NECC) near 10°N and hence less annual variation in the strength of the NECC. It is interesting that both the steric height and SSS have less annual variability in Argo than in WOA01 at 9°N, suggesting that interannual variability in the atmospheric annual cycle forcing may be responsible. In Fig. 4.10 the Argo annual cycle in steric height also appears more regular (less noisy) on the equator and farther south.

5. Discussion and conclusion

The temporal mean ocean temperature and salinity fields and the annual cycle for the period 2004–2008 have been estimated from Argo data in order to compare the Argo era with historical data and to examine Argo's annual cycle for consistency with related global ocean surface measurements. Argo data alone were used to construct the gridded dataset analyzed in this study, in order to test the array's stand-alone capabilities, to ensure that the present estimates are not biased toward earlier data, and to ensure that they are not contaminated by mixing of instrument types. Stable estimates of the mean and annual cycle were obtained from a first estimate based on a weighted least-squares fit to the temperature and salinity data, followed by objective analysis of monthly anomalies using statistics derived from sample correlation estimates.

It is important to recognize that a longer averaging period with the full Argo array is desirable, even though the errors in the mean are already smaller than the differences between it and historical climatologies. There remain some regions with insufficient Argo sampling, potentially leading to biases in the mean field, especially near ocean boundaries and south of 50°S (Fig. 2.1). In these regions the mean remains sensitive to the details of the estimation technique until more data are available. More uniform coverage in the array will improve estimation of both the mean and the time-variability. Errors in estimates of low frequency variability can result from biases in the mean field in the presence of evolving data coverage. For example, if the estimated mean in the Southern Ocean has a warm bias, then increasing numbers of Argo floats in that region would produce a spurious appearance of cooling. Such systematic errors are seldom considered even though they may be large.

Comparison of the Argo era to the WOA01 historical hydrographic climatology (Conkright et al., 2002) emphasized that multi-decadal warming extending into the deep ocean is seen in both

hemispheres at middle and high latitudes. The Southern Ocean warming is distributed across all three oceans and may include both a downward and a southward displacement of isotherms. It is accompanied by a freshening signal along pressure and density surfaces that correspond to Sub-Polar Mode Water and Antarctic Intermediate Water. The northern warming is mainly in the North Atlantic, and is accompanied by a salinity increase of fairly recent origin. The near-surface ocean is warmer at all latitudes than the historical climatology. Its salinity is increased at middle (evaporative) latitudes and mostly decreased in regions of excess P − E.

Argo's annual cycle appears consistent with the NOAA OI SST product (Reynolds et al., 2002) for the same 2004–2008 period, with the NOC air–sea heat flux climatology (Josey et al., 1998), and with gridded satellite altimetric height (Ducet et al., 2000). Some interesting differences were identified in all of these comparisons that may be attributable to ocean processes, or to interannual variability or systematic errors. The differences indicate a need for more detailed comparative studies that are beyond the scope of this work.

Error estimates were made for both the mean and variability in steric height, based on subsampling experiments that use satellite altimetry. These indicated that the Argo-minus-WOA differences are greater than Argo sampling errors. With respect to large-scale (seasonal, thousand kilometer) variability, Argo sampling was found to have good signal-to-noise characteristics at low latitudes, as expected, but with a need for improved sampling in the Southern Ocean. It was noted that increased interannual variability will emerge when the Argo mean is extended over a longer period of time.

Two additional error estimates for large-scale variability were made, first by dividing the Argo dataset randomly into two groups of floats and comparing gridded estimates from the separate groups, and second by comparing Argo near-surface temperature with the independent NOAA OI SST product. As with altimetric height subsampling, these experiments indicated highest signal-to-noise ratio in the tropics, and had similar variation in latitude of the magnitudes of signal and noise. From these two experiments, the globally averaged variance of large-scale ($10^\circ \times 10^\circ \times 3$ months) steric height error was less than 1 dyn cm^2, and the error variance in large-scale SST was about 0.05 $^\circ C^2$.

In any time-series study, it is tempting to wait for a longer dataset. Despite the limitations of the present Argo time-series, it is essential to begin Argo analysis now for several important reasons.

(1) The Argo array continues to evolve, and should do so effectively. Questions of how well the array is performing in relation to its initial design studies (Roemmich et al., 1998) are central to continuing and improving the array for its goal of sampling large-scale ocean variability.
(2) The present Argo dataset is a better representation of the modern upper ocean than is any historical climatology, especially in the southern hemisphere. The improvement in the mean fields resulting from a few incremental years of sampling will be smaller than the contrasts to historical data. Argo is already demonstrating its value in studies of climate variability and change.
(3) The systematic pressure error in a subset of Argo floats discussed in Section 2 was discovered through scientific analysis of the data (Willis et al., 2007) rather than by the formal quality control process. Careful data analyses are needed to identify any remaining problems too subtle for the QC system, and to develop improved QC tools. Climatologies are powerful tools for QC.
(4) A key activity for global ocean observations is their use in ocean data assimilating models for ocean state estimation and prediction. While these models include errors, their characterization, typically as white noise, does not allow for bias errors in the data types that are assimilated. It is important to investigate the consistency of the ocean observing system through conventional statistical comparisons.

Other recent studies have estimated interannual variability and trends in globally averaged Argo temperature or steric height (e.g. Willis et al., 2008; Cazenave et al., 2009). These are important issues, but the Argo dataset will take some years, and careful comparison to all available shipboard CTD measurements, to achieve its best quality and to have that quality assessed. The studies to date demonstrate that there is still substantial uncertainty in closure of the sea level budget on the 5-year timescale for which Argo, satellite altimetry, and satellite gravimetry presently overlap. A longer period of time is needed both to analyze and reduce the systematic errors in these measurements, and for the modest trends in the component estimates to stand out above the remaining errors.

We plan to continue developing estimation techniques for interpolating the global Argo dataset, to update the mean and monthly gridded product, and to compare it with other Argo-based estimates and related datasets. The present 60-month global time-series together with comparable products from other authors using different dataset selection, QC procedures and estimation techniques, are being noted on Argo web sites (see http://www.argo.net). We believe that comparative effort by interested investigators around the world is the best pathway toward improvement of the Argo dataset, its products, and its scientific utilization. Argo's open data policy is an invitation for everyone to join the Argo analysis initiative.

Acknowledgements

The Argo data used here were collected and are made freely available by the International Argo Program and by the national programs that contribute to it. Analysis was supported in part by the NASA *JASON-1* project through JPL Contract 961424 to SIO. The authors and their part of the Argo project were supported by U.S. Argo through NOAA Grant NA17RJ1231 (SIO–JIMO). The statements, findings, conclusions, and recommendations herein are those of the authors and do not necessarily reflect the views of the National Oceanic and Atmospheric Administration or the Department of Commerce. The efforts of many international partners in planning and implementing the Argo array are gratefully acknowledged. Graphics were produced using Ferret software, a product of NOAA's Pacific Marine Environmental Laboratory. The AVISO altimeter products were produced by the CLS Space Oceanography Division as part of the Environment and Climate EU ENACT project (EVK2-CT2001-00117) and with support from CNES. Valuable comments on the manuscript were provided by P. Sutton.

References

Bindoff, N., McDougall, T., 1994. Diagnosing climate change and ocean ventilation using hydrographic data. Journal of Physical Oceanography 24, 1137–1152.
Bretherton, F., Davis, R., Fandry, C., 1976. A technique for objective analysis of oceanographic experiments applied to MODE-73. Deep-Sea Research, 23559–23582.
Cazenave, A., Dominh, K., Guienhut, S., Berthier, E., Llovel, W., Ramillien, G., Ablain, M., Larnicol, G., 2009. Sea level budget over 2003–2008: a reevaluation from GRACE space gravimetry, satellite altimetry and Argo. Global and Planetary Change 65, 83–88.
Chambers, D.P., Wahr, J., Nerem, R.S., 2004. Preliminary observations of global ocean mass variations with GRACE. Geophysical Research Letters 31, L13310. doi:10.1029/2004GL020461.
Chen, J.L., Wilson, C.R., Chambers, D.P., 1998. Seasonal global water mass balance and mean sea level variations. Geophysical Research Letters 25, 3555–3558.

Curry, R., Dickson, B., Yushaev, I., 2003. A change in the freshwater balance of the Atlantic Ocean over the past four decades. Nature 426, 826–829.
Conkright, M.E., Locarnini, R.A., Garcia, H.E., O'Brien, T.D., Boyer, T.P., Stephens, C., Antonov, J.I., 2002. World Ocean Atlas 2001: Objective Analyses, Data Statistics, and Figures, CD-ROM Documentation. National Oceanographic Data Center, Silver Spring, MD. 17 pp.
Davis, R., 1998. Preliminary results from directly measuring middepth circulation in the tropical and South Pacific. Journal of Geophysical Research 103, 24619–24639.
Domingues, C.M., Church, J.A., White, N.J., Gleckler, P., Wijffels, S.E., Barker, P.M., Dunn, J.R., 2008. Improved estimates of upper-ocean warming and multi-decadal sea-level rise. Nature 453, 1090–1093.
Ducet, N., Le Traon, P.-Y., Reverdin, G., 2000. Global high resolution mapping of ocean circulation from TOPEX/Poseidon and ERS-1 and -2. Journal of Geophysical Research 105 (C8), 19477–19498.
Gill, A., Niiler, P., 1973. The theory of the seasonal variability in the ocean. Deep-Sea Research 20, 141–177.
Gille, S., 2008. Decadal-scale temperature trends in the southern hemisphere ocean. Journal of Climate 21, 4749–4765.
Gilson, J., Roemmich, D., Cornuelle, B., 1998. Relationship of TOPEX/Poseidon altimetric height to steric height and circulation in the North Pacific. Journal of Geophysical Research 103, 27947–27965.
Gouretski, V.V., Koltermann, K.P., 2004. WOCE – Global Hydrographic Climatology. Berichte des Bundesamtes für Seeschifffahrt und Hydrographie, Technical Report 35/2004, 50 pp.
Gouretski, V., Koltermann, K.P., 2007. How much is the ocean really warming? Geophysical Research Letters 34, L01610. doi:10.1029/2006GL027834.
Gregory, J., Banks, H., Stott, P., Lowe, J., Palmer, M., 2004. Simulated and observed decadal variability in ocean heat content. Geophysical Research Letters 31, L15312. doi:10.1029/2004GL020258.
Hadfield, R.E., Wells, N.C., Josey, S.A., Hirschi, J.J.-M., 2007. On the accuracy of North Atlantic temperature and heat storage fields from Argo. Journal of Geophysical Research 112, C01009. doi:10.1029/2006JC003825.
Hatun, H., Sando, A., Drange, H., Hansen, B., Valdimarsson, H., 2005. Influence of the Atlantic subpolar gyre on the thermohaline circulation. Science 309, 1841–1844.
Ishii, M., Kimoto, M., Sakamoto, K., Iwasaki, S.-I., 2006. Steric sea level changes estimated from historical ocean subsurface temperature and salinity analyses. Journal of Oceanography 62, 155–170.
Johnson, G.C., Sloyan, B., Kessler, W., McTaggert, K., 2002. Direct measurements of upper ocean currents and water properties across the tropical Pacific during the 1990s. Progress in Oceanography 52, 31–61.
Josey, S.A., Kent, E.C., Taylor, P.K., 1998. The Southampton Oceanography Centre (SOC) Ocean – Atmosphere Heat, Momentum and Freshwater Flux Atlas. Southampton Oceanography Centre Report No. 6, 30 pp.
Lavender, K.L., Owens, W.B., Davis, R.E., 2005. The mid-depth circulation of the subpolar North Atlantic Ocean as measured by subsurface floats. Deep-Sea Research Part I: Oceanographic Research Papers 52 (5), 767–785.
Levitus, S., 1986. Annual cycle of salinity and salt storage in the World Ocean. Journal of Physical Oceanography 16, 322–343.
Levitus, S., Antonov, J., 1997. Climatological and Interannual Variability of Temperature, Heat Storage, and Rate of Heat Storage in the Upper Ocean, NOAA NESDIS Atlas 16. U.S. Government Printing Office, Washington, DC, 6 pp. and 186 Figs.
Levitus, S., Monterey, G.I., Boyer, T., 1997. Seasonal Variability of Dynamic Height and its Fourier Analysis. NOAA NESDIS Atlas 15, U.S. Government Printing Office, Washington, DC, 9 pp. and 38 Figs.
Levitus, S., Antonov, J., Boyer, T., 2005a. Warming of the world ocean, 1955–2003. Geophysical Research Letters 32, L02604. 10.1029/2004GL021592. Online data at <http://www.nodc.noaa.gov/OC5/DATA_ANALYSIS/heat_intro.html>.
Levitus, S., Antonov, J.I., Boyer, T.P., Garcia, H.E., Locarnini, R.A., 2005b. Linear trends of zonally averaged thermosteric, halosteric, and steric sea level changes for individual ocean basins and the world ocean, (1955–1959)–(1994–1998). Geophysical Research Letters 32, L16601. doi:10.1029/2005GL023761.
Moisan, J., Niiler, P., 1998. The seasonal heat budget of the North Pacific: net heat flux and heat storage rates (1950–1990). Journal Physical Oceanography 28, 401–421.
Owens, W.B., Wong, A.P.S., 2009. An improved calibration method for the drift of the conductivity sensor on autonomous CTD profiling floats by theta-S climatology. Deep-Sea Research Part I: Oceanographic Research Papers 56 (3), 450–457.
Reid, J.L., 1986. On the total geostrophic circulation of the south Pacific Ocean: flow patterns, tracers, and transports. Progress in Oceanography 16, 1–61.
Reid, J.L., 2003. On the total geostrophic circulation of the Indian Ocean: flow patterns, tracers and transports. Progress in Oceanography 56, 137–186.
Reynolds, R.W., Rayner, N.A., Smith, T.M., Stokes, D.C., Wang, W., 2002. An improved in situ and satellite SST analysis for climate. Journal of Climate 15, 1609–1625.
Ridgway, K.R., Dunn, J.R., Wilkin, J.L., 2002. Ocean interpolation by four-dimensional weighted least squares – application to the waters around Australasia. Journal of Atmospheric and Oceanic Technology 19, 1357–1375.
Ridgway, K.R., Dunn, J.R., 2007. Observational evidence for a southern hemisphere oceanic supergyre. Geophysical Research Letters 34, L13612. doi:10.1029/2007GL030392.
Roemmich, D., 1983. Optimal estimation of hydrographic station data and derived fields. Journal of Physical Oceanography 13, 1544–1549.
Roemmich, D., Sutton, P., 1998. The mean and variability of ocean circulation past northern New Zealand: Determining the representativeness of hydrographic climatologies. Journal of Geophysical Research 103, 13041–13054.
Roemmich, D., et al. (the Argo Science Team), 1998. On the design and implementation of Argo: an initial plan for a global array of profiling floats. International CLIVAR Project Office Report 21, GODAE Report 5. GODAE International Project Office, Melbourne, Australia, 32 pp.
Roemmich, D., Gilson, J., Davis, R., Sutton, P., Wijffels, S., Riser, S., 2007. Decadal spin-up of the South Pacific subtropical gyre. Journal of Physical Oceanography 37 (2), 162–173.
Speich, S., Blanke, B., deVries, P., Drijfhout, S., Doos, K., Ganachaud, A., Marsh, R., 2002. Tasman leakage: a new route in the global ocean conveyor belt. Geophysical Research Letters 29. doi:10.1029/2001GL014586.
White, W., 1995. Design of a global observing system for gyre-scale upper ocean temperature variability. Progress in Oceanography 36, 169–217.
White, W., Tai, C.-K., 1995. Inferring interannual changes in global upper ocean heat storage from TOPEX altimetry. Journal of Geophysical Research 100 (C12), 24943–24954.
Wijffels, S.E., Willis, J., Domingues, C.M., Barker, P., White, N.J., Gronell, A., Ridgway, K., Church, J.A., 2008. Changing expendable bathythermograph fall rates and their impact on estimates of thermosteric sea level rise. Journal of Climate. 21, 5657–5672.
Willis, J.K., Chambers, D.P., Nerem, R.S., 2008. Assessing the globally averaged sea level budget on seasonal to interannual timescales. Journal of Geophysical Research 113, C06015. doi:10.1029/2007JC004517.
Willis, J.K., Lyman, J.M., Johnson, G.C., Gilson, J., 2007. Correction to Recent cooling of the upper ocean. Geophysical Research Letters 34, L16601. doi:10.1029/2007GL030323.
Willis, J.K., Roemmich, D., Cornuelle, B., 2004. Interannual variability in upper ocean heat content, temperature, and thermosteric expansion on global scales. Journal of Geophysical Research 109, C12036. doi:10.1029/2003JC002260.
Wong, A., Bindoff, N., Church, J., 1999. Large-scale freshening of intermediate waters in the Pacific and Indian Oceans. Nature 400, 440–443.
Wong, A.P.S., Johnson, G.C., Owens, W.B., 2003. Delayed-mode calibration of autonomous CTD profiling float salinity data by theta-S climatology. Journal of Atmospheric and Atmospheric Technology 20 (2), 308–318.
Wyrtki, K., 1974. Sea level and the seasonal fluctuations of the equatorial currents in the western Pacific Ocean. Journal of Physical Oceanography 4, 91–103.
Zang, X., Wunsch, C., 2001. Spectral description of low-frequency oceanic variability. Journal of Physical Oceanography 31, 3073–3095.